POLITECNICO DI TORINO
Repository ISTITUZIONALE

Observation of deuteron and antideuteron formation from resonance-decay nucleons

Original
Observation of deuteron and antideuteron formation from resonance-decay nucleons / Null, N., Acharya, S., Agarwal, A., Aglieri Rinella, G., Aglietta, L., Agnello, M., Agrawal, N., Ahammed, Z., Ahmad, S., Ahn, S.U., Ahuja, I., Akindinov, A., Akishina, V., Al-Turany, M., Aleksandrov, D., Alessandro, B., Alfanda, H.M., Alfaro Molina, R., Ali, B., Alici, A., et al.. - In: NATURE. - ISSN 0028-0836. - 648:8093(2025), pp. 306-311. [10.1038/s41586-025-09775-5]

Availability:
This version is available at: 11583/3016099 since: 2026-09-29T20:25:05Z

Publisher:
Springer Nature

Published
DOI:10.1038/s41586-025-09775-5

Terms of use:

This article is made available under terms and conditions as specified in the corresponding bibliographic description in the repository

Publisher copyright

(Article begins on next page)

26 November 2026

Article

Observation of deuteron and antideuteron formation from resonance-decay nucleons

https://doi.org/10.1038/s41586-025-09775-5

Received: 7 May 2025

Accepted: 20 October 2025

Published online: 10 December 2025

Open access

Check for updates

The ALICE Collaboration* ✉

High-energy hadronic collisions generate environments characterized by temperatures above 100 MeV (refs. 1,2), about 100,000 times hotter than the centre of the Sun. At present, it is therefore unclear how light (anti)nuclei with mass number A of a few units, such as the deuteron, ^{3}He or ^{4}He, each bound by only a few MeV, can emerge from these collisions[3,4]. Here, the ALICE Collaboration reports that deuteron–pion momentum correlations in proton–proton (pp) collisions provide model-independent evidence that about 90% of the observed (anti)deuterons are produced in nuclear reactions[5] following the decay of short-lived resonances, such as the Δ(1232). These findings, obtained by the ALICE Collaboration at the Large Hadron Collider, resolve a gap in our understanding of nucleosynthesis in ultrarelativistic hadronic collisions. Apart from offering insights on how (anti)nuclei are formed in hadronic collisions, the results can be used in the modelling of the production of light and heavy nuclei in cosmic rays[6] and dark-matter decays[7,8].

Nuclear physicists have long been intrigued by the microscopic mechanism behind the formation of light nuclei and antinuclei in hadron–hadron collisions[3,4]. In ultrarelativistic heavy-ion collisions with energies per nucleon up to a few TeV (10^{12} eV), the study of particle production is directly connected to the confinement of colour charge in colour-neutral hadrons. These collisions produce a quark–gluon plasma, a state in which quarks and gluons are deconfined, and as the system evolves, they bind into hadrons and light (anti)nuclei[1,9]. As the binding energies of light (anti)nuclei are substantially lower (2.23 MeV for deuteron, 7.72 MeV for ^{3}He; ref. 10) than the average kinetic energy of hadrons in these energetic collisions (of the order of 100 MeV; ref. 1), the question is about both the formation of loosely bound nuclei and their survival through the hadronic phase that follows the hadronization of the quark–gluon plasma. This issue is also relevant in ultrarelativistic proton–proton (pp) and proton–nucleus (p–A) collisions, in which the formation of a quark–gluon plasma remains under experimental and theoretical scrutiny and average kinetic energies above 100 MeV can still be achieved[2].

The study of (anti)nucleus formation in hadronic collisions is of importance in astrophysics. On one front, the precise composition of ultrahigh-energy (>PeV) cosmic rays, particularly their heavier elements ($A > 50$) component, remains an open question[6]. A microscopic modelling of nucleus formation in ultrarelativistic hadron collisions is an essential ingredient for understanding the composition of these cosmic rays and for uncovering the origin of particle acceleration mechanisms in the Universe[11]. On another front, antinuclei formation—whether from cosmic-ray interactions with the interstellar medium or as potential products of dark-matter decay—plays a pivotal part in indirect searches for dark matter[7,8,12]. Experimental investigations into the microscopic processes underlying light nucleus and antinucleus formation thus offer a dual benefit: they advance the knowledge of the strong interaction in the non-perturbative regime and provide the quantitative framework needed to decode the spectra of cosmic rays and their origins.

The yields of nuclei such as deuterons (p–n bound system), ^{3}H (p–n–n), ^{3}He (p–p–n), ^{4}He (p–p–n–n), $^3_\Lambda$H (Λ–p–n) and their corresponding antinuclei have been precisely measured at the Relativistic Heavy Ion Collider in Au–Au collisions at centre-of-mass energies per nucleon pair ($\sqrt{s_{NN}}$) across an energy range of 7.7–200 GeV (refs. 13–16) and at the Large Hadron Collider (LHC) for pp collisions at $\sqrt{s}$ ranging from 0.9 TeV to 13 TeV, as well as for p–Pb and Pb–Pb collisions at $\sqrt{s_{NN}} = 2.76$–8.16 TeV (refs. 17–20). Current understanding suggests that nuclei can be produced either through direct emission as multi-quark states following a collision, similar to other hadrons such as protons or pions, or through a secondary binding mechanism of nucleons.

Two types of models have been used to study these mechanisms. Statistical hadronization models describe the direct production and assume that hadrons and nuclei are directly emitted from a source in thermal and chemical equilibrium, with abundances determined by the particle mass, the system temperature, volume and quantum number conservation[9,21,22]. This work uses the canonical statistical model (CSM)[23], which is better suited for pp collisions. Although CSMs predict yields effectively, they do not provide insights into the microscopic mechanisms driving (anti)nucleus formation. By contrast, coalescence models[12,24–27] emulate binding mechanisms and they assume that (anti) nucleons form independently before binding to create (anti)nuclei. This approach incorporates microscopic parameters, such as the spatial proximity of nucleons alongside their strong interactions, allowing for a satisfactory description of yields and momentum distributions[25,28].

Microscopic calculations implemented in event generators for heavy-ion collisions[5,29] include pion-catalysed reactions—both formation and disintegration (for example, $\pi + p + n \Leftrightarrow \pi + d$)—and successfully describe measured nuclear yields. The important aspect of these models is that a third body, such as a meson, aids the binding process by carrying away the excess energy.

Overall a direct experimental evidence for the microscopic mechanisms of (anti)nucleus formation remains unknown. Femtoscopy

*A list of authors and their affiliations appears at the end of the paper. ✉e-mail: alice-publications@cern.ch

provides a complementary approach by examining pion–(anti)deuteron (π–d) momentum correlations and offers direct insights into the microscopic processes underlying (anti)deuteron formation. This technique has been effectively used by the ALICE Collaboration to study various hadron pairs produced in pp and p–Pb collisions at the LHC, see for example, ref. 30 and the references therein, shedding light on their residual strong interactions.

Using π–d femtoscopy correlations, the study presented in this paper shows, in a model-independent manner, that (anti)deuterons are formed following the decay of strong resonances, such as the Δ(1232) (hereafter Δ). Considering the possible contribution to all produced resonances, we estimate that 88.9 ± 6.3% of the observed (anti)deuterons are generated through binding processes. These findings resolve a longstanding puzzle regarding the formation of light (anti)nuclei in collider experiments and provide a robust foundation for further modelling of nucleosynthesis from hadronic collisions, both in accelerators and in the Universe.

Resonances and correlation function

As a bound state of a proton and a neutron, the deuteron may inherit correlations developed by its constituent nucleons during the evolution of the collision. The study of π–d correlations offers a sensitive probe of this process. If deuterons are produced thermally alongside pions, any correlation signal between them would arise solely from final-state interactions. By contrast, if deuterons form through the coalescence of nucleons originating from the decay of an intermediate resonance, the resulting π–d correlation function could retain the signatures of that resonance.

The correlation function $C(k^*)$ is the key experimental observable, and k^* is the single-particle momentum in the pair rest frame (PRF). Experimentally, $C(k^*) = \mathcal{N}[N_{\text{same}}(k^*)/N_{\text{mixed}}(k^*)]$, where $N_{\text{same}}(k^*)$ (same-event sample) is the distribution of relative momenta between the π–d pair measured for pions and deuterons stemming from the same collision[31]. Equivalently, $N_{\text{mixed}}(k^*)$ (mixed-event sample) is an uncorrelated reference obtained by building the distribution through the combination of pions and deuterons originating from different collisions. Finally, $\mathcal{N}$ is a normalization factor ensuring the proper convergence of $C(k^*)$ to unity at large k^*. In the case of non-interacting particles, the correlation function is equal to unity for all k^* as the relative momentum distribution is purely governed by the underlying single-particle phase space, which is the same for $N_{\text{same}}(k^*)$ and $N_{\text{mixed}}(k^*)$ distributions. An attractive interaction enhances the correlation function above unity at low $k^* \lesssim 200$ MeV c^{-1}, whereas a repulsive interaction leads to a depletion below unity. A resonance that decays into the hadron pair of interest would produce a peak in the k^* spectrum.

Figure 1 shows three scenarios of (anti)deuteron production mechanisms and interactions and the resulting $\pi^{\pm}$–d correlations. Simulations were performed to quantify the effects of the different production scenarios, and details are provided in the Methods. All scenarios include repulsive (red curves) and attractive (green curves) Coulomb interactions for the π^+–d and π^-–d systems, respectively. The strong interaction contribution is minimal because of the small scattering parameters of the $\pi^{\pm}$–d system and is hence neglected[32,33]. In the first two scenarios (Fig. 1a,b), directly produced deuterons and pions are considered. The simulation results shown on the right were obtained assuming that pions and (anti)deuterons are produced following a canonical statistical hadronization scheme, ThermalFIST[34]. The obtained correlation functions are multiplied by the Coulomb correlation function. The results indicate a depletion in the correlation function at low k^* for π^+–d and an enhancement for π^-–d because of the Coulomb interaction.

In Fig. 1b, the elastic and inelastic scattering of pions and deuterons is considered. This is tested by using the hadronic transport model SMASH[35] as an afterburner to ThermalFIST to simulate inelastic and elastic rescattering according to the experimental cross-sections. The

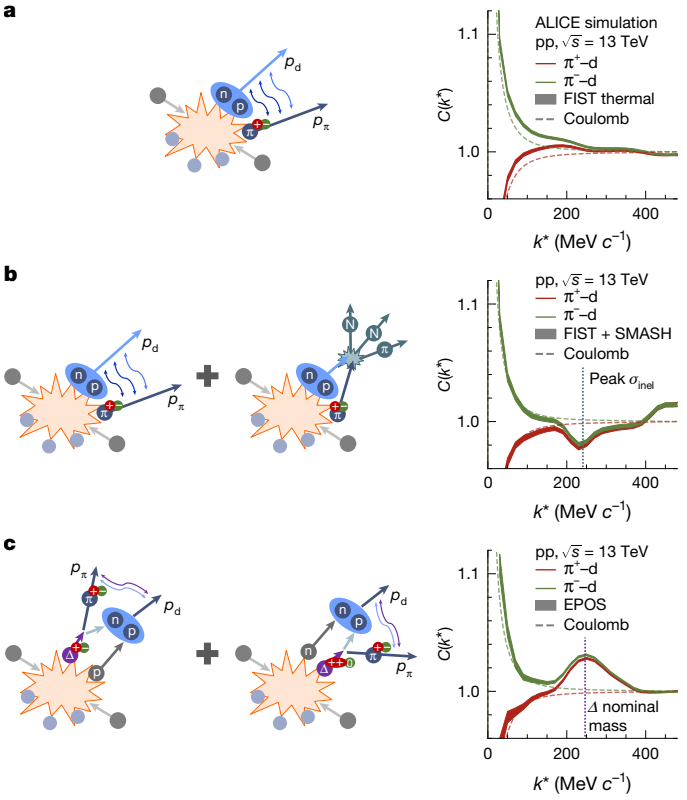

Fig. 1 | (Anti)deuteron production scenarios. Illustration of three scenarios for deuteron production and interaction with pions (left) and the resulting $\pi^{\pm}$–d correlation functions (right). All scenarios include Coulomb attraction between π^-–d (green curves) and Coulomb repulsion between the π^+–d (red curves). The dashed lines always show the correlation function using Coulomb interaction. **a**,**b**, Thermally produced deuterons with only Coulomb (**a**) and Coulomb + elastic + inelastic (**b**) interactions, respectively. **c**, Deuteron formation by nuclear binding following Δ-resonance decays. All the simulations include the charge conjugates ($\pi^+ - d \equiv \pi^+ - d \oplus \pi^- - \bar{d}$ and $\pi^- - d \equiv \pi^- - d \oplus \pi^+ - \bar{d}$). The bandwidths corresponds to the statistical uncertainties of the models.

elastic processes do not modify the shape of the correlation function, as both the incoming and outgoing $\pi^{\pm}$–d pairs must conserve energy, ensuring that their relative momentum k^* remains unchanged. The same holds for pseudo-elastic processes, in which an intermediate Δ resonance is formed, as in π + (pn) → pΔ → π + (pn).

By contrast, inelastic $\pi^{\pm}$–d scattering leads to deuteron destruction, reducing the number of measurable pairs in the k^* region in which the inelastic cross-section reaches its maximum. Both elastic and inelastic cross-sections peak at the nominal Δ mass ($k^* \approx 240$ MeV c^{-1}), and the inelastic one is three times larger than the elastic contribution[36]. Figure 1b (right) shows the results of these simulations for the π^+–d and π^-–d cases. As expected, a depletion at the relative momentum $k^* \approx 240$ MeV c^{-1}, corresponding to the peak of the inelastic cross-section, is observed.

In Fig. 1c, a deuteron forms when a primordial nucleon binds with one from a Δ decay. These resonances are very short-lived excited states of nucleons and decay after approximately 1.5 fm c^{-1} into π–nucleon pairs. Considering all charge states ($\Delta^{++,+,0,-}$), they are expected to contribute 43% of the nucleon yield in pp collisions at the LHC[34,37]. Measurements of the $\pi^{\pm}$–p femtoscopy correlations by ALICE[38] have already shown the presence of the Δ resonances, modified by rescattering and regeneration effects (Methods). For the formation of deuterons, the possible combinations include neutron–proton binding from $\Delta^{++} \to \pi^+$–p or $\Delta^0 \to \pi^-$–p, proton–neutron binding from $\Delta^+ \to \pi^{\pm}$–n, and binding of two nucleons from separate Δ decays. This scenario was simulated by

exploiting a state-of-the-art coalescence afterburner[25] combined with the EPOS 3 event generator[39,40]. The latter accounts for resonance production and their decays, whereas the aforementioned rescattering and regeneration effects are not included in the simulations. The results are shown in the right panel, and a clear peak appears in correspondence with the Δ resonance nominal mass. The observed peak is due to the residual correlation between the pion and an (anti)nucleon from the Δ decay during the (anti)deuteron formation process.

The three patterns in the correlation function correspond to different physics scenarios and are easily distinguishable from one another. The observed patterns remain unchanged across different models: although model parametrization may shift or rescale the structures, their shapes are preserved. This constitutes a solid reference to proceed with the interpretation of the experimental data.

Discussion

The experimental π^+–d and π^-–d correlation functions have been measured in pp collisions at $\sqrt{s} = 13$ TeV. Charged pions ($\pi^{\pm}$), deuteron (d) and antideuteron ($\bar{\mathrm{d}}$) tracks are reconstructed with the ALICE detector, and their momentum transverse to the beam direction (p_{T}) is measured in the range $p_{\mathrm{T}} \in [0.14, 4.0]$ GeV c^{-1} for pions and $p_{\mathrm{T}} \in [0.8, 2.4]$ GeV c^{-1} for deuterons. The excellent particle identification and tracking abilities of the ALICE detector provide samples of π^+ (π^-) and d ($\bar{\mathrm{d}}$) with a purity of 99% and 100%, respectively. Further details on the particle selection and evaluation of the systematic uncertainties are described in the Methods. After the selection of pions and (anti)deuterons, the correlation functions for pairs of particles (π^+–d and π^-–d) and their charge conjugates ($\pi^+ - \bar{\mathrm{d}}$ and $\pi^- - \bar{\mathrm{d}}$) are obtained. As the same interaction governs hadron–hadron and antihadron–antihadron pairs[31], the sum of particles and antiparticles is considered ($\pi^+ - \mathrm{d} \equiv \pi^+ - \mathrm{d} \oplus \pi^- - \bar{\mathrm{d}}$ and $\pi^- - \mathrm{d} \equiv \pi^- - \mathrm{d} \oplus \pi^+ - \bar{\mathrm{d}}$) in the following. The resulting π^-–d and π^+–d correlation functions are shown by the open markers in Fig. 2a,b. The grey boxes around the markers represent the systematic uncertainties, and the vertical bars show the statistical uncertainties. The fit results for the π^-–d and π^+–d correlation functions are shown in Fig. 2a,b, respectively.

The measured $\pi^{\pm}$–d correlation functions are modelled and fitted using a decomposition approach summarized by the relation $C_{\mathrm{fit}}(k^*) = \varepsilon(k^*) \otimes B(k^*)[\lambda_{\mathrm{gen}} C_{\mathrm{gen}}(k^*) + (1 - \lambda_{\mathrm{gen}})]$ (Methods). Here, $\varepsilon(k^*)$ represents a correction for momentum resolution effects, and $B(k^*)$ is a baseline accounting for residual background correlations. The latter arise mainly from non-primary pions produced in weak decays of long-lived resonances, as well as from secondary particles originating from interactions with the detector material. These contributions can mimic correlated pairs and must be accounted for in the modelling. The parameter λ_{gen} quantifies the fraction of genuine $\pi^{\pm}$–d pairs, with the non-genuine component primarily arising from the feed-down of long-lived resonances into pions[41] with a lifetime $\tau > 5$ fm c^{-1}. The term $C_{\mathrm{gen}}(k^*)$ denotes the corresponding genuine correlation function that contains Coulomb and strong interactions, alongside contributions from the Δ resonance. The interaction components are modelled using the CATS (Correlation Analysis Tool using the Schrödinger equation) framework[42]. Theoretically, $C(k^*) = \int \mathrm{d}^3 r^* S(r^*) \times |\psi(\mathbf{k}^*, \mathbf{r}^*)|^2$, where r^* is the relative distance (in the PRF) between the particles at the time of their effective emission, $\psi(\mathbf{k}^*, \mathbf{r}^*)$ is the wavefunction of the pair relative motion, and $S(r^*)$ is the source function corresponding to the probability to emit the pair at a certain relative distance r^* (ref. 43). Dedicated studies of the source function in pp collisions at $\sqrt{s} = 13$ TeV performed by the ALICE Collaboration showed a common emission source for all hadrons[38,41,44]. This source is typically modelled by a Gaussian function with a standard deviation (an effective size of the source) of $r_{\mathrm{eff}} \approx 1.5$ fm, obtained by accounting for the contribution of short-lived resonances (see Methods for details).

For the source, an effective Gaussian distribution with $r_{\mathrm{eff}} = 1.51 \pm 0.12$ fm was used (Methods). The real part of the π^-–d potential is included in the fit. However, owing to the small scattering parameters of the $\pi^{\pm}$–d system, the contribution is negligible[32,33]. To gauge the influence of the resonance decays on the $\pi^{\pm}$–d correlations, the contributions of the Δ resonances extracted from the measured $\pi^{\pm}$–p correlations are modified assuming that the nucleon emerging from the Δ decay coalesces with an additional nucleon to form a deuteron. The assumption is that the two nucleons have similar momenta (see Methods for details). Finally, the relative momentum k^* between the pion from the Δ decay and the deuteron is evaluated. All charge states $\Delta^{++,+,0,-}$ are considered, assuming the $\Delta^{+,-}$ peak has the same shape as $\Delta^{++,0}$ from $\pi^{\pm}$–p correlations. The experimental correlation functions are well described, confirming the scenario in which the deuteron is formed after the decay of the Δ by a fusion process as assumed in Fig. 1c. An excellent description (Fig. 2) of the measured correlation function is

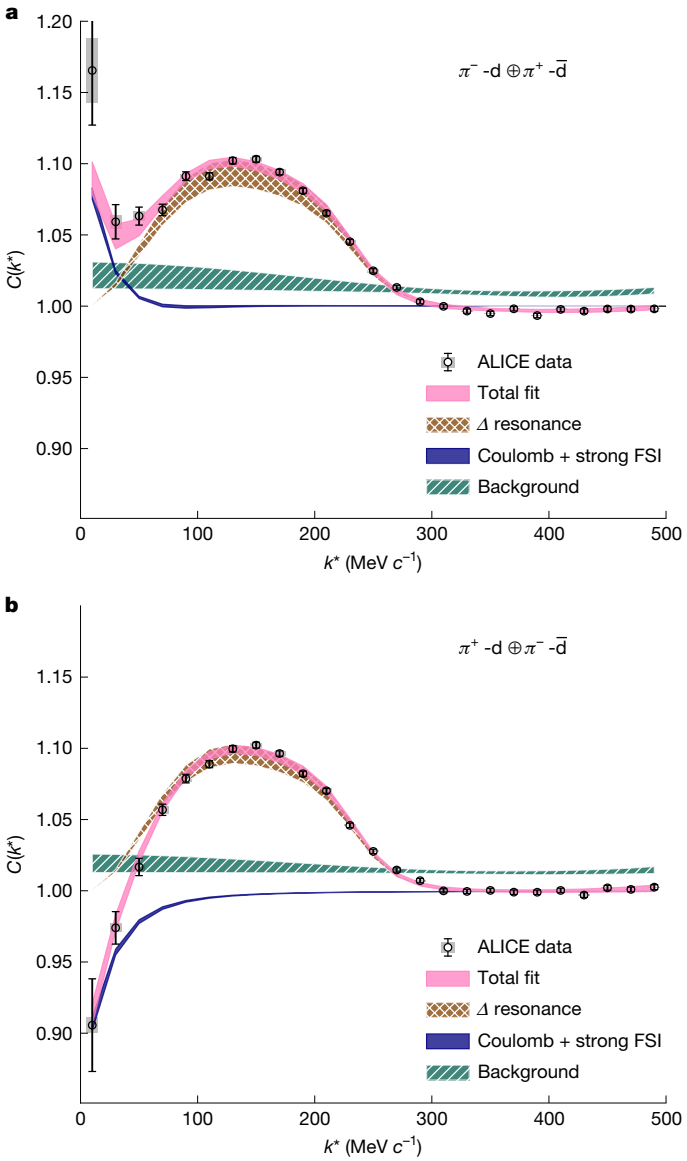

Fig. 2 | Experimental π^-–d and π^+–d correlation functions. The data are obtained from high-multiplicity pp collisions at $\sqrt{s} = 13$ TeV. **a**, The measured π^-–d correlation function together with the corresponding fit function (magenta). The brown cross-hatched band represents contributions from the Δ resonance, the blue band denotes the Coulomb and strong FSI interactions, and the teal diagonally hatched band corresponds to the residual background. The widths of the bands indicate the fit uncertainty. **b**, In the same representation, the π^+–d correlation function. However, the strong FSI interaction is neglected for this system. The χ^2 per degree of freedom is 14/15 for both correlations.

obtained by adopting the data-driven shape of the Δ derived from $\pi^{\pm}$–p correlations[38]. The Δ shape in the $\pi^{\pm}$–d correlation function exhibits a shift towards lower masses due to rescattering effects, consistent with the displacement observed in Fig. 2 relative to the nominal Δ position at $k^* \approx 240$ MeV c^{-1}. The simulations obtained with the EPOS 3 event generator at present do not include the rescattering of the Δ decay products, resulting in no shift of the Δ peak in Fig. 1c.

The evidence of Δ decay in the $\pi^{\pm}$–d correlation function is model-independent, as freeing the radius parameter does not affect the results, the Coulomb interaction is inherently model-independent and the residual background is accounted for in the systematic uncertainties of the fit.

Furthermore, the fraction of deuterons produced following a resonance decay is extracted. The contribution from Δ resonances is evaluated by integrating the peak in the $\pi^{\pm}$–d correlation functions corresponding to these resonances, subtracting the number of $\pi^{\pm}$–d pairs expected in the same k^* region without a nucleon originating from the Δ resonance (Coulomb + background) and dividing the result by the total number of detected deuterons. The result is corrected for combinatorial effects, reconstruction efficiency and the non-measured π^0 final state. With these corrections, the fraction of deuterons produced by a Δ resonance is calculated to be 60.6 ± 4.1% (Methods). To test the compatibility of this measurement with expectations from event generators, the EPOS 3 model is used. For this, the yield of baryonic resonances in EPOS 3 was adjusted to match the predictions of the CSM ThermalFIST for pp collisions at $\sqrt{s} = 13$ TeV. Furthermore, the change in the pion detector acceptance resulting from the shift in the experimentally observed Δ spectral shape is taken into account. In this simulation, the fraction of deuteron for which at least one of the nucleons stems from any Δ resonance and both the deuteron and the π are found within the acceptance is determined to be 53.8 ± 3.1% (more details in the Methods). The fact that these two fractions are in agreement within 1.32 standard deviations demonstrates that the survival probability of deuterons produced in pp collisions at the LHC is very high. This is the case because (anti)nuclei are produced after the resonance decays, in which spectral temperatures of about 20 MeV (see the Methods for details) have been evaluated, much lower than the average kinetic energy of hadrons (about 100 MeV) in pp collisions at the LHC.

Deuterons can form through fusion after any strong resonance decay, with Δ resonances accounting for 77.3 ± 1.2% of all cases. Moreover, considering that 15.5 ± 0.5% of Δ resonances are not properly reconstructed because of the detector acceptance effects, the experimental fraction of deuterons from Δ can be scaled up to a total fraction of deuterons originating from all resonances of 88.9 ± 6.3%. These results indicate not only that the presence of resonances can contribute to the (anti) deuteron production but also that it is the dominant process responsible for the creation of deuterons.

Summary

In this work, $\pi^{\pm}$–d correlation functions measured in pp collisions at $\sqrt{s} = 13$ TeV by the ALICE Collaboration at the LHC are used to study the (anti)deuteron production mechanism. It is demonstrated that (anti) deuteron formation by nucleonic fusion follows the strong decay of short-lived resonances. Model-independent evidence is provided by observing the residual correlation of pion–nucleon pairs stemming from the same Δ decay in the pion–deuteron correlation function. This effect can be explained only assuming that (anti)deuteron formation occurs after the Δ decay and the measured correlation is interpreted by a data-driven method based on the independent measurement of the Δ in the $\pi^{\pm}$–p final state. The residual signal in the $\pi^{\pm}$–d correlations can be used to evaluate the fraction of (anti)deuterons produced following Δ decays, which is found to be 60.6 ± 4.1%. Extending this reasoning to all strong resonances produced in pp collisions at $\sqrt{s} = 13$ TeV, it is found that 88.9 ± 6.3% of (anti)deuterons are formed through binding processes involving nucleons originating from strongly decaying resonances. This large fraction demonstrates that most of the (anti) nuclei are produced through secondary binding processes in pp collisions at the LHC and not by direct emission as other hadrons. A large survival probability is expected for (anti)deuterons as the low spectral temperature of Δ (about 20 MeV) reflects that the environment in which (anti)nuclei are created is characterized by a much lower kinetic energies than the hadronization phase (around 100 MeV) in pp collisions at the LHC. These findings solve a longstanding puzzle in nuclear physics, providing insight into the microscopic mechanism that leads to (anti) nuclei formation in pp collisions at the LHC. These insights can now be used for a more realistic microscopic modelling of (anti)nuclei production, for example, in reactions induced by cosmic ray.

Online content

Any methods, additional references, Nature Portfolio reporting summaries, source data, extended data, supplementary information, acknowledgements, peer review information; details of author contributions and competing interests; and statements of data and code availability are available at https://doi.org/10.1038/s41586-025-09775-5.

1. ALICE Collaboration. The ALICE experiment: a journey through QCD. *Eur. Phys. J. C* **84**, 813 (2024).
2. ALICE Collaboration. Multiplicity dependence of π, *K*, and p production in pp collisions at $\sqrt{s}$=13 TeV. *Eur. Phys. J. C* **80**, 693 (2020).
3. Butler, S. T., & Pearson, C. A. Deuterons from high-energy proton bombardment of matter. *Phys. Rev.* **129**, 836–842 (1963).
4. Kapusta, J. I. Mechanisms for deuteron production in relativistic nuclear collisions. *Phys. Rev. C* **21**, 1301–1310 (1980).
5. Sun, K.-J., Wang, R., Ko, C. M., Ma, Y.-G. & Shen, C. Unveiling the dynamics of little-bang nucleosynthesis. *Nat. Commun.* **15**, 1074 (2024).
6. Pierre Auger Collaboration. Depth of maximum of air-shower profiles at the Pierre Auger Observatory. I. Measurements at energies above $10^{17.8}$ eV. *Phys. Rev. D* **90**, 122005 (2014).
7. ALICE Collaboration. Measurement of anti-^{3}He nuclei absorption in matter and impact on their propagation in the Galaxy. *Nat. Phys.* **19**, 61–71 (2023).
8. Šerkšnytė, L. et al. Reevaluation of the cosmic antideuteron flux from cosmic-ray interactions and from exotic sources. *Phys. Rev. D* **105**, 083021 (2022).
9. Andronic, A., Braun-Munzinger, P., Redlich, K. & Stachel, J. Decoding the phase structure of QCD via particle production at high energy. *Nature* **561**, 321–330 (2018).
10. Marcucci, L. E. et al. The hyperspherical harmonics method: a tool for testing and improving nuclear interaction models. *Front. Phys.* **8**, 10.3389/fphy.2020.00069 (2020).
11. Petrosian, V. & Bykov, A. Particle acceleration mechanisms. *Space Sci. Rev.* **134**, 207–227 (2008).
12. Kachelrieß, M., Ostapchenko, S. & Tjemsland, J. Alternative coalescence model for deuteron, tritium, helium-3 and their antinuclei. *Eur. Phys. J. A* **56**, 4 (2020).
13. PHENIX Collaboration. Deuteron and antideuteron production in Au+Au collisions at $\sqrt{s_{NN}}$=200 GeV. *Phys. Rev. Lett.* **94**, 122302 (2005).
14. BRAHMS Collaboration. Rapidity dependence of deuteron production in central Au+Au collisions at $\sqrt{s_{NN}}$=200 GeV. *Phys. Rev. C* **83**, 044906 (2011).
15. STAR Collaboration. Observation of an antimatter hypernucleus. *Science* **328**, 58–62 (2010).
16. STAR Collaboration. Observation of the antimatter helium-4 nucleus. *Nature* **473**, 353–356 (2011).
17. ALICE Collaboration. Production of light nuclei and anti-nuclei in pp and Pb–Pb collisions at energies available at the CERN Large Hadron Collider. *Phys. Rev. C* **93**, 024917 (2016).
18. ALICE Collaboration. Multiplicity dependence of (anti-)deuteron production in pp collisions at $\sqrt{s}$=7 TeV. *Phys. Lett. B* **794**, 50–63 (2019).
19. ALICE Collaboration. Multiplicity dependence of light (anti-)nuclei production in p-Pb collisions at $\sqrt{s_{NN}}$=5.02 TeV. *Phys. Lett. B* **800**, 135043 (2020).
20. ALICE Collaboration. Production of (anti-)^{3}He and (anti-)^{3}H in p–Pb collisions at $\sqrt{s_{NN}}$=5.02 TeV. *Phys. Rev. C* **101**, 044906 (2020).
21. Andronic, A., Braun-Munzinger, P., Stachel, J. & Stöcker, H. Production of light nuclei, hypernuclei and their antiparticles in relativistic nuclear collisions. *Phys. Lett. B* **697**, 203–207 (2011).
22. Dönigus, B., Röpke, G. & Blaschke, D. Deuteron yields from heavy-ion collisions at energies available at the CERN Large Hadron Collider: continuum correlations and in-medium effects. *Phys. Rev. C* **106**, 044908 (2022).
23. Vovchenko, V., Dönigus, B. & Stoecker, H. Canonical statistical model analysis of p–p, p–Pb, and Pb–Pb collisions at energies available at the CERN Large Hadron Collider. *Phys. Rev. C* **100**, 054906 (2019).
24. Blum, K. & Takimoto, M. Nuclear coalescence from correlation functions. *Phys. Rev. C* **99**, 044913 (2019).
25. Mahlein, M. et al. A realistic coalescence model for deuteron production. *Eur. Phys. J. C* **83**, 804 (2023).
26. Mrowczynski, S. Deuteron formation mechanism. *J. Phys. G* **13**, 1089–1098 (1987).
27. Mrówczyński, S. & Słoń, P. Hadron–deuteron correlations and production of light nuclei in relativistic heavy-ion collisions. *Acta Phys. Polon. B* **51**, 1739–1755 (2020).
28. Aichelin, J. et al. Parton-hadron-quantum-molecular dynamics: a novel microscopic *n*-body transport approach for heavy-ion collisions, dynamical cluster formation, and hypernuclei production. *Phys. Rev. C* **101**, 044905 (2020).

29. Neidig, T., Gallmeister, K., Greiner, C., Bleicher, M. & Vovchenko, V. Towards solving the puzzle of high temperature light (anti)-nuclei production in ultra-relativistic heavy ion collisions. *Phys. Lett. B* **827**, 136891 (2022).
30. ALICE Collaboration. Exploring the strong interaction of three-body systems at the LHC. *Phys. Rev. X* **14**, 031051 (2024).
31. ALICE Collaboration., S. Acharya et al. p–p, p–Λ and Λ–Λ correlations studied via femtoscopy in pp reactions at √s=7 TeV. *Phys. Rev. C* **99**, 024001 (2019).
32. Meissner, U.-G., Raha, U. & Rusetsky, A. The pion-nucleon scattering lengths from pionic deuterium. *Eur. Phys. J. C* **41**, 213–232 (2005).
33. Hauser, P. et al. New precision measurement of the pionic deuterium s-wave strong interaction parameters. *Phys. Rev. C* **58**, R1869–R1872 (1998).
34. Vovchenko, V. & Stoecker, H. Thermal-FIST: a package for heavy-ion collisions and hadronic equation of state. *Comput. Phys. Commun.* **244**, 295–310 (2019).
35. Petersen, H. et al. SMASH – a new hadronic transport approach. *Nucl. Phys. A* **982**, 399–402 (2019).
36. Coci, G. et al. Dynamical mechanisms for deuteron production at mid-rapidity in relativistic heavy-ion collisions from energies available at the GSI Schwerionensynchrotron to those at the BNL Relativistic Heavy Ion Collider. *Phys. Rev. C* **108**, 014902 (2023).
37. Vovchenko, V., & Stoecker, H. Analysis of hadron yield data within hadron resonance gas model with multi-component eigenvolume corrections. *J. Phys. Conf. Ser.* **779**, 012078 (2017).
38. ALICE Collaboration. Investigating the p–π± and p–p–π± dynamics with femtoscopy in pp collisions at √s=13 TeV. *Eur. Phys. J. A* **61**, 194 (2025).
39. Werner, K., Karpenko, I., Pierog, T., Bleicher, M. & Mikhailov, K. Event-by-event simulation of the three-dimensional hydrodynamic evolution from flux tube initial conditions in ultrarelativistic heavy ion collisions. *Phys. Rev. C* **82**, 044904 (2010).
40. Werner, K., Guiot, B., Karpenko, I. & Pierog, T. Analysing radial flow features in p-Pb and p-p collisions at several TeV by studying identified particle production with the event generator EPOS3. *Phys. Rev. C* **89**, 064903 (2014).
41. ALICE Collaboration. Common femtoscopic hadron-emission source in pp collisions at the LHC. *Eur. Phys. J. C* **85**, 198 (2025).
42. Mihaylov, D. et al. A femtoscopic correlation analysis tool using the Schrödinger equation (CATS). *Eur. Phys. J. C* **78**, 394 (2018).
43. Lisa, M. et al. Femtoscopy in relativistic heavy-ion collisions: two decades of progress. *Ann. Rev. Nucl. Part. Sci.* **55**, 357–402 (2005).
44. ALICE Collaboration. Corrigendum to "Search for a common baryon source in high-multiplicity pp collisions at the LHC" [Phys. Lett. B 811 (2020) 135849]. *Phys. Lett. B* **861**, 139233 (2025).

Publisher's note Springer Nature remains neutral with regard to jurisdictional claims in published maps and institutional affiliations.

Open Access This article is licensed under a Creative Commons Attribution 4.0 International License, which permits use, sharing, adaptation, distribution and reproduction in any medium or format, as long as you give appropriate credit to the original author(s) and the source, provide a link to the Creative Commons licence, and indicate if changes were made. The images or other third party material in this article are included in the article's Creative Commons licence, unless indicated otherwise in a credit line to the material. If material is not included in the article's Creative Commons licence and your intended use is not permitted by statutory regulation or exceeds the permitted use, you will need to obtain permission directly from the copyright holder. To view a copy of this licence, visit http://creativecommons.org/licenses/by/4.0/.

© The Author(s) 2025

The ALICE Collaboration

S. Acharya[1], A. Agarwal[2], G. Aglieri Rinella[3], L. Aglietta[4], M. Agnello[5], N. Agrawal[6], Z. Ahammed[2], S. Ahmad[7], S. U. Ahn[8], I. Ahuja[9], A. Akindinov[10], V. Akishina[11], M. Al-Turany[12], D. Aleksandrov[10], B. Alessandro[13], H. M. Alfanda[14], R. Alfaro Molina[15], B. Ali[7], A. Alici[6], N. Alizadehvandchali[16], A. Alkin[17], J. Alme[18], G. Alocco[4], T. Alt[19], A. R. Altamura[1], I. Altsybeev[20], J. R. Alvarado[21], M. N. Anaam[14], C. Andrei[22], N. Andreou[23], A. Andronic[24], E. Andronov[10], V. Anguelov[25], F. Antinori[26], P. Antonioli[27], N. Apadula[28], H. Appelshäuser[19], C. Arata[29], S. Arcelli[6], R. Arnaldi[13], J. G. M. C. A. Arneiro[30], I. C. Arsene[31], M. Arslandok[32], A. Augustinus[3], R. Averbeck[12], D. Averyanov[10], M. D. Azmi[7], H. Baba[33], A. Badalà[34], J. Bae[17], Y. Bae[17], Y. W. Baek[35], X. Bai[36], R. Bailhache[19], Y. Bailung[37], R. Bala[38], A. Baldisseri[39], B. Balis[40], S. Bangalia[41], Z. Banoo[38], V. Barbasova[9], F. Barile[42], L. Barioglio[13], M. Barlou[43], B. Barman[44], G. G. Barnaföldi[45], L. S. Barnby[23], E. Barreau[46], V. Barret[47], L. Barreto[30], K. Barth[3], E. Bartsch[19], N. Bastid[47], S. Basu[48], G. Batigne[46], D. Battistini[20], B. Batyunya[49], D. Bauri[50], J. L. Bazo Alba[51], I. G. Bearden[52], P. Becht[12], D. Behera[37], I. Belikov[53], A. D. C. Bell Hechavarria[24], F. Bellini[6], R. Bellwied[16], S. Belokurova[10], L. G. E. Beltran[54], Y. A. V. Beltran[21], G. Bencedi[45], A. Bensaoula[16], S. Beole[4], Y. Berdnikov[10], A. Berdnikova[25], L. Bergmann[25], L. Bernardinis[55], L. Betev[3], P. P. Bhaduri[2], T. Bhalla[56], A. Bhasin[38], B. Bhattacharjee[44], S. Bhattarai[41], L. Bianchi[4], J. Bielčík[57], J. Bielčková[58], A. P. Bigot[53], A. Bilandzic[20], A. Binoy[41], G. Biro[45], S. Biswas[59], N. Bize[46], D. Blau[10], M. B. Blidaru[12], N. Bluhme[11], C. Blume[19], F. Bock[60], T. Bodova[18], J. Bok[61], L. Boldizsár[45], M. Bombara[9], P. M. Bond[3], G. Bonomi[62,63], H. Borel[39], A. Borissov[10], A. G. Borquez Carcamo[25], E. Botta[4], Y. E. M. Bouziani[19], D. C. Brandibur[64], L. Bratrud[19], P. Braun-Munzinger[12], M. Bregant[30], M. Broz[57], G. E. Bruno[42,65], V. D. Buchakchiev[66], M. D. Buckland[67], D. Budnikov[10], H. Buesching[19], S. Bufalino[5], P. Buhler[68], N. Burmasov[10], Z. Buthelezi[69,70], A. Bylinkin[18], S. A. Bysiak[71], J. C. Cabanillas Noris[54], M. F. T. Cabrera[16], H. Caines[32], A. Caliva[72], E. Calvo Villar[51], J. M. M. Camacho[54], P. Camerini[55], M. T. Camerlingo[1], F. D. M. Canedo[30], S. Cannito[55], S. L. Cantway[32], M. Carabas[73], F. Carnesecchi[3], L. A. D. Carvalho[30], J. Castillo Castellanos[39], M. Castoldi[3], F. Catalano[3], S. Cattaruzzi[55], R. Cerri[4], I. Chakaberia[28], P. Chakraborty[74], S. Chandra[2], S. Chapeland[3], M. Chartier[75], S. Chattopadhay[2], M. Chen[76], T. Cheng[14], C. Cheshkov[77], D. Chiappara[78], V. Chibante Barroso[3], D. D. Chinellato[68], F. Chinu[4], E. S. Chizzali[20,141], J. Cho[79], S. Cho[79], P. Chochula[3], Z. A. Chochulska[74], D. Choudhury[44], S. Choudhury[80], P. Christakoglou[81], C. H. Christensen[52], P. Christiansen[48], T. Chujo[82], M. Ciacco[5], C. Cicalo[83], G. Cimador[4], F. Cindolo[27], M. R. Ciupek[12], G. Clai[27,142], F. Colamaria[1], J. S. Colburn[84], D. Colella[42], A. Colelli[42], M. Colocci[6], M. Concas[3], G. Conesa Balbastre[29], Z. Conesa del Valle[85], G. Contin[55], J. G. Contreras[57], M. L. Coquet[46], P. Cortese[13,86], M. R. Cosentino[87], F. Costa[3], S. Costanza[88], P. Crochet[47], M. M. Czarnynoga[74], A. Dainese[26], G. Dange[11], M. C. Danisch[25], A. Danu[64], P. Das[3], S. Das[59], A. R. Dash[24], S. Dash[50], A. De Caro[72], G. de Cataldo[1], J. de Cuveland[11], A. De Falco[89], D. De Gruttola[72], N. DeMarco[13], C. De Martin[55], S. DePasquale[72], R. Deb[62], R. DelGrande[20], L. Dello Stritto[3], G. G. A. de Souza[30,143], P. Dhankher[90], D. DiBari[42], M. Di Costanzo[5], A. Di Mauro[3], B. Di Ruzza[91], B. Diab[3], R. A. Diaz[49], Y. Ding[14], J. Ditzel[19], R. Divià[3], Ø. Djuvsland[18], U. Dmitrieva[10], A. Dobrin[64], B. Dönigus[19], J. M. Dubinski[74], A. Dubla[12], P. Dupieux[47], N. Dzalaiova[92], T. M. Eder[24], R. J. Ehlers[28], F. Eisenhut[19], R. Ejima[93], D. Elia[1], B. Erazmus[46], F. Ercolessi[6], B. Espagnon[85], G. Eulisse[3], D. Evans[84], S. Evdokimov[10], L. Fabbietti[20], M. Faggin[3], J. Faivre[29], F. Fan[14], W. Fan[28], T. Fang[14], A. Fantoni[94], M. Fasel[60], G. Feofilov[10], A. Fernández Téllez[21], L. Ferrandi[30], M. B. Ferrer[3], A. Ferrero[39], C. Ferrero[13,144], A. Ferretti[4], V. J. G. Feuillard[25], V. Filova[57], D. Finogeev[10], F. M. Fionda[83], F. Flor[32], A. N. Flores[95], S. Foertsch[69], I. Fokin[25], S. Fokin[10], U. Follo[13,144], E. Fragiacomo[96], E. Frajna[45], H. Fribert[20], U. Fuchs[3], N. Funicello[72], C. Furget[29], A. Furs, T. Fusayasu[97], J. J. Gaardhøje[52], M. Gagliardi[4], A. M. Gago[51], T. Gahlaut[50], C. D. Galvan[54], S. Gami[98], D. R. Gangadharan[16], P. Ganoti[43], C. Garabatos[12], J. M. Garcia[21], T. García Chávez[21], E. Garcia-Solis[99], S. Garetti[85], C. Gargiulo[3], P. Gasik[12], H. M. Gaur[11], A. Gautam[41], M. B. Gay Ducati[100], M. Germain[46], R. A. Gernhaeuser[20], C. Ghosh[2], M. Giacalone[27], G. Gioachin[5], S. K. Giri[2], P. Giubellino[12,13], P. Giubilato[78], A. M. C. Glaenzer[39], P. Glässel[25], E. Glimos[101], V. Gonzalez[102], P. Gordeev[10], M. Gorgon[40], K. Goswami[37], S. Gotovac[103], V. Grabski[15], L. K. Graczykowski[74], E. Grecka[58], A. Grelli[104], C. Grigoras[3], V. Grigoriev[10], S. Grigoryan[49,105], O. S. Groettvik[3], F. Grosa[3], J. F. Grosse-Oetringhaus[3], R. Grosso[12], D. Grund[57], N. A. Grunwald[25], R. Guernane[29], M. Guilbaud[46], K. Gulbrandsen[52], J. K. Gumprecht[68], T. Gündem[19], T. Gunji[33], J. Guo[106], W. Guo[14], A. Gupta[38], R. Gupta[38], R. Gupta[37], K. Gwizdziel[74], L. Gyulai[45], C. Hadjidakis[85], F. U. Haider[38], S. Haidlova[57], M. Haldar[59], H. Hamagaki[107], Y. Han[108], B. G. Hanley[102], R. Hannigan[95], J. Hansen[48], J. W. Harris[32], A. Harton[99], M. V. Hartung[19], H. Hassan[109], D. Hatzifotiadou[27], P. Hauer[110], L. B. Havener[32], E. Hellbär[3], H. Helstrup[111], M. Hemmer[19], T. Herman[57], S. G. Hernandez[16], G. Herrera Corral[112], S. Herrmann[77], K. F. Hetland[111], B. Heybeck[19], H. Hillemanns[3], B. Hippolyte[53], I. P. M. Hobus[81], F. W. Hoffmann[113], B. Hofman[104], A. Horzyk[40], Y. Hou[14], P. Hristov[3], P. Huhn[19], L. M. Huhta[109], T. J. Humanic[114], A. Hutson[16], D. Hutter[11], M. C. Hwang[90], R. Ilkaev[10], M. Inaba[82], M. Ippolitov[10], A. Isakov[81], T. Isidori[41], M. S. Islam[50], S. Iurchenko[10], M. Ivanov[12], M. Ivanov[92], V. Ivanov[10], K. E. Iversen[48], M. Jablonski[40], B. Jacak[28,90], N. Jacazio[6], P. M. Jacobs[28], S. Jadlovska[115], J. Jadlovsky[115], S. Jaelani[116], C. Jahnke[117], M. J. Jakubowska[74], M. A. Janik[74], S. Ji[61], S. Jia[106], T. Jiang[106], A. A. P. Jimenez[118], S. Jin[106], F. Jonas[28], D. M. Jones[75], J. M. Jowett[3,12], J. Jung[19], M. Jung[19], A. Junique[3], A. Jusko[84], J. Kaewjai[119], P. Kalinak[120], A. Kalweit[3], A. Karasu Uysal[121], N. Karatzenis[84], O. Karavichev[10], T. Karavicheva[10], E. Karpechev[10], M. J. Karwowska[74], U. Kebschull[113], M. Keil[3], B. Ketzer[110], J. Keul[19], S. S. Khade[37], A. M. Khan[36], S. Khan[7], A. Khanzadeev[10], Y. Kharlov[10], A. Khatun[41], A. Khuntia[57], Z. Khuranova[19], B. Kileng[111], B. Kim[17], C. Kim[61], D. J. Kim[109], D. Kim[17], E. J. Kim[122], G. Kim[79], H. Kim[79], J. Kim[108], J. Kim[79], J. Kim[3,122], M. Kim[90], S. Kim[123], T. Kim[108], K. Kimura[93], S. Kirsch[19], I. Kisel[11], S. Kiselev[10], A. Kisiel[74], J. L. Klay[124], J. Klein[3], S. Klein[28], C. Klein-Bösing[24], M. Kleiner[19], T. Klemenz[20], A. Kluge[3], C. Kobdaj[119], R. Kohara[33], T. Kollegger[12], A. Kondratyev[49], N. Kondratyeva[10], J. Konig[19], S. A. Konigstorfer[20], P. J. Konopka[3], G. Kornakov[74], M. Korwieser[20], S. D. Koryciak[40], C. Koster[81], A. Kotliarov[58], N. Kovacic[125], V. Kovalenko[10], M. Kowalski[71], V. Kozhuharov[66], G. Kozlov[11], I. Králik[120], A. Kravčáková[9], L. Krcal[3], M. Krivda[84,120], F. Krizek[58], K. Krizkova Gajdosova[57], C. Krug[100], M. Krüger[19], D. M. Krupova[57], E. Kryshen[10], V. Kučera[79], C. Kuhn[53], P. G. Kuijer[81], T. Kumaoka[82], D. Kumar[2], L. Kumar[56], N. Kumar[56], S. Kumar[1], S. Kundu[3], M. Kuo[82], P. Kurashvili[126], A. B. Kurepin[10], A. Kuryakin[10], S. Kushpil[58], V. Kuskov[10], M. Kutyla[74], A. Kuznetsov[49], M. J. Kweon[79], Y. Kwon[108], S. L. LaPointe[11], P. LaRocca[127], A. Lakrathok[119], M. Lamanna[3], S. Lambert[46], A. R. Landou[29], R. Langoy[128], P. Larionov[3], E. Laudi[3], L. Lautner[20], R. A. N. Laveaga[54], R. Lavicka[68], R. Lea[62,63], H. Lee[17], I. Legrand[22], G. Legras[24], A. M. Lejeune[57], T. M. Lelek[40], R. C. Lemmon[67], I. León Monzón[54,148], M. M. Lesch[20], P. Lévai[45], M. Li[14], P. Li[106], X. Li[106], B. E. Liang-Gilman[90], J. Lien[128], R. Lietava[84], I. Likmeta[16], B. Lim[4], H. Lim[61], S. H. Lim[61], S. Lin[106], V. Lindenstruth[11], C. Lippmann[12], D. Liskova[115], D. H. Liu[14], J. Liu[75], G. S. S. Liveraro[117], I. M. Lofnes[18], C. Loizides[60], S. Lokos[71], J. Lömker[104], X. Lopez[47], E. López Torres[129], C. Lotteau[77], P. Lu[12,36], W. Lu[14], Z. Lu[106], F. V. Lugo[15], J. Luo[76], G. Luparello[96], M. A. T. Johnson[21], Y. G. Ma[76], M. Mager[3], M. Mahlein[20], A. Maire[53], E. M. Majerz[40], M. V. Makariev[66], M. Malaev[10], G. Malfattore[6,27], N. M. Malik[38], N. Malik[7], S. K. Malik[38], D. Mallick[85], N. Mallick[109], G. Mandaglio[34,130], S. K. Mandal[126], A. Manea[64], V. Manko[10], A. K. Manna[37], F. Manso[47], G. Mantzaridis[20], V. Manzari[1], Y. Mao[14], R. W. Marcjan[40], G. V. Margagliotti[55], A. Margotti[27], A. Marn[12], C. Markert[95], P. Martinengo[3], M. I. Martínez[21], G. Martínez García[46], M. P. P. Martins[3,30], S. Masciocchi[12], M. Masera[4], A. Masoni[83], L. Massacrier[85], O. Massen[104], A. Mastroserio[1,91], L. Mattei[4,47], S. Mattiazzo[78], A. Matyja[71], F. Mazzaschi[3], M. Mazzilli[16], Y. Melikyan[131], M. Melo[30], A. Menchaca-Rocha[15], J. E. M. Mendez[118], E. Meninno[68], A. S. Menon[16], M. W. Menzel[3,25], M. Meres[92], L. Micheletti[13], D. Mihai[73], D. L. Mihaylov[20,66], A. U. Mikalsen[18], K. Mikhaylov[10,49], N. Minafra[41], D. Miśkowiec[12], A. Modak[62,96], B. Mohanty[98], M. Mohisin Khan[7,145], M. A. Molander[131], M. M. Mondal[98], S. Monira[74], C. Mordasini[109], D. A. Moreira DeGodoy[24], I. Morozov[10], A. Morsch[3], T. Mrnjavac[3], V. Muccifora[94], S. Muhuri[2], A. Mulliri[89], M. G. Munhoz[30], R. H. Munzer[19], H. Murakami[33], L. Musa[3], J. Musinsky[120], J. W. Myrcha[74], N. B. Sundstrom[104], B. Naik[70], A. I. Nambrath[90], B. K. Nandi[50], R. Nania[27], E. Nappi[1], A. F. Nassirpour[123], V. Nastase[73], A. Nath[25], N. F. Nathanson[52], C. Nattrass[101], K. Naumov[90], M. N. Naydenov[66], A. Neagu[31], L. Nellen[118], R. Nepeivoda[48], S. Nese[31], N. Nicassio[42], B. S. Nielsen[52], E. G. Nielsen[52], S. Nikolaev[10], V. Nikulin[10], F. Noferini[27], S. Noh[132], P. Nomokonov[49], J. Norman[75], N. Novitzky[60], J. Nystrand[18], M. R. Ockleton[75], M. Ogino[107], S. Oh[123], A. Ohlson[48], V. A. Okorokov[10], J. Oleniacz[74], C. Oppedisano[13], A. Ortiz Velasquez[118], J. Otwinowski[71], M. Oya[93], K. Oyama[107], S. Padhan[50], D. Pagano[62,63], G. Paić[118], S. Paisano-Guzmán[21], A. Palasciano[1], I. Panasenko[48], S. Panebianco[39], P. Panigrahi[50], C. Pantouvakis[78], H. Park[82], J. Park[82], S. Park[17], J. E. Parkkila[3], Y. Patley[50], R. N. Patra[1], P. Paudel[41], B. Paul[2], H. Pei[14], T. Peitzmann[104], X. Peng[133], M. Pennisi[4], S. Perciballi[4], D. Peresunko[10], G. M. Perez[129], Y. Pestov[10], V. Petrov[10], M. Petrovici[22], S. Piano[96], M. Pikna[92], P. Pillot[46], O. Pinazza[3,27], L. Pinsky[16], C. Pinto[3], S. Pisano[94], M. Płoskoń[28], M. Planinic[125], D. K. Plociennik[40], M. G. Poghosyan[60], B. Polichtchouk[10], S. Politano[3,4], N. Poljak[125], A. Pop[22], S. Porteboeuf-Houssais[47], I. Y. Pozos[21], K. K. Pradhan[37], S. K. Prasad[59], S. Prasad[37],

R. Preghenella[27], F. Prino[13], C. A. Pruneau[102], I. Pshenichnov[10], M. Puccio[3], S. Pucillo[4], L. Quaglia[4], A. M. K. Radhakrishnan[37], S. Ragoni[134], A. Rai[32], A. Rakotozafindrabe[39], N. Ramasubramanian[77], L. Ramello[13,86], C. O. Ramírez-Álvarez[21], M. Rasa[127], S. S. Räsänen[131], R. Rath[27], M. P. Rauch[18], I. Ravasenga[3], K. F. Read[60,101], C. Reckziegel[87], A. R. Redelbach[11], K. Redlich[126,146], C. A. Reetz[12], H. D. Regules-Medel[21], A. Rehman[18], F. Reidt[3], H. A. Reme-Ness[111], K. Reygers[25], A. Riabov[10], V. Riabov[10], R. Ricci[72], M. Richter[18], A. A. Riedel[20], W. Riegler[3], A. G. Riffero[4], M. Rignanese[78], C. Ripoli[72], C. Ristea[64], M. V. Rodriguez[3], M. Rodríguez Cahuantzi[21], K. Røed[31], R. Rogalev[10], E. Rogochaya[49], D. Rohr[3], D. Röhrich[18], S. Rojas Torres[57], P. S. Rokita[74], G. Romanenko[6], F. Ronchetti[3], D. Rosales Herrera[21], E. D. Rosas[118], K. Roslon[74], A. Rossi[26], A. Roy[37], S. Roy[50], N. Rubini[27], J. A. Rudolph[81], D. Ruggiano[74], R. Rui[55], P. G. Russek[40], R. Russo[81], A. Rustamov[135], E. Ryabinkin[10], Y. Ryabov[10], A. Rybicki[71], L. C. V. Ryder[41], J. Ryu[61], W. Rzesa[74], B. Sabiu[27], S. Sadhu[110], S. Sadovsky[10], J. Saetre[18], S. Saha[98], B. Sahoo[37], R. Sahoo[37], D. Sahu[37], P. K. Sahu[136], J. Saini[2], K. Sajdakova[9], S. Sakai[82], S. Sambyal[38], D. Samitz[68], I. Sanna[3,20], T. B. Saramela[30], D. Sarkar[52], P. Sarma[44], V. Sarritzu[89], V. M. Sarti[20], M. H. P. Sas[3], S. Sawan[98], E. Scapparone[27], J. Schambach[60], H. S. Scheid[3,19], C. Schiaua[22], R. Schicker[25], F. Schlepper[3,25], A. Schmah[12], C. Schmidt[12], M. O. Schmidt[3], M. Schmidt[137], N. V. Schmidt[60], A. R. Schmier[101], J. Schoengarth[19], R. Schotter[68], A. Schröter[11], J. Schukraft[3], K. Schweda[12], G. Scioli[6], E. Scomparin[13], J. E. Seger[134], Y. Sekiguchi[33], D. Sekihata[33], M. Selina[81], I. Selyuzhenkov[12], S. Senyukov[53], J. J. Seo[25], D. Serebryakov[10], L. Serkin[118,147], L. Šerkšnytė[20], A. Sevcenco[64], T. J. Shaba[69], A. Shabetai[46], R. Shahoyan[3], A. Shangaraev[10], B. Sharma[38], D. Sharma[50], H. Sharma[26], M. Sharma[38], S. Sharma[38], T. Sharma[44], U. Sharma[38], A. Shatat[85], O. Sheibani[102], K. Shigaki[93], M. Shimomura[138], S. Shirinkin[10], Q. Shou[76], Y. Sibiriak[10], S. Siddhanta[83], T. Siemiarczuk[126], T. F. Silva[30], D. Silvermyr[48], T. Simantathammakul[119], R. Simeonov[66], B. Singh[38], B. Singh[20], K. Singh[37], R. Singh[98], R. Singh[12,26], S. Singh[7], V. K. Singh[2], V. Singhal[2], T. Sinha[80], B. Sitar[92], M. Sitta[13,86], T. B. Skaali[31], G. Skorodumovs[25], N. Smirnov[32], R. J. M. Snellings[104], E. H. Solheim[31], C. Sonnabend[3,12], J. M. Sonneveld[81], F. Soramel[78], A. B. Soto-Hernandez[114], R. Spijkers[81], I. Sputowska[71], J. Staa[48], J. Stachel[25], I. Stan[64], T. Stellhorn[24], S. F. Stiefelmaier[25], D. Stocco[46], I. Storehaug[31], N. J. Strangmann[19], P. Stratmann[24], S. Strazzi[6], A. Sturniolo[34,130], C. P. Stylianidis[81], A. A. P. Suaide[30], C. Suire[85], A. Suiu[3,73], M. Sukhanov[10], M. Suljic[3], R. Sultanov[10], V. Sumberia[38], S. Sumowidagdo[116], L. H. Tabares[129], S. F. Taghavi[20], J. Takahashi[117], G. J. Tambave[98], Z. Tang[36], J. Tanwar[56], J. D. Tapia Takaki[41], N. Tapus[73], L. A. Tarasovicova[9], M. G. Tarzila[22], A. Tauro[3], A. Tavira García[85], G. Tejeda Muñoz[21], L. Terlizzi[4], C. Terrevoli[1], D. Thakur[4], S. Thakur[59], M. Thogersen[31], D. Thomas[95], A. Tikhonov[10], N. Tiltmann[3,24], A. R. Timmins[16], M. Tkacik[115], A. Toia[19], R. Tokumoto[93], S. Tomassini[6], K. Tomohiro[93], N. Topilskaya[10], M. Toppi[94], V. V. Torres[46], A. Trifiró[34,130], T. Triloki[65], A. S. Triolo[3.34,130], S. Tripathy[3], T. Tripathy[47], S. Trogolo[4], V. Trubnikov[139], W. H. Trzaska[109], T. P. Trzcinski[74], C. Tsolanta[31], R. Tu[76], A. Tumkin[10], R. Turrisi[26], T. S. Tveter[31], K. Ullaland[18], B. Ulukutlu[20], S. Upadhyaya[71], A. Uras[77], M. Urioni[55], G. L. Usai[89], M. Vaid[38], M. Vala[9], N. Valle[63], L. V. R. van Doremalen[104], M. van Leeuwen[81], C. A. vanVeen[25], R. J. G. van Weelden[81], D. Varga[45], Z. Varga[32], P. Vargas Torres[118], M. Vasileiou[43], A. Vasiliev[10,148], O. Vázquez Doce[94], O. Vazquez Rueda[16], V. Vechernin[10], P. Veen[39], E. Vercellin[4], R. Verma[50], R. Vértesi[45], M. Verweij[104], L. Vickovic[103], Z. Vilakazi[70], O. Villalobos Baillie[84], A. Villani[55], A. Vinogradov[10], T. Virgili[72], M. M. O. Virta[109], A. Vodopyanov[49], B. Volkel[3], M. A. Völkl[84], S. A. Voloshin[102], G. Volpe[42], B. vonHaller[3], I. Vorobyev[3], N. Vozniuk[10], J. Vrláková[9], J. Wan[76], C. Wang[76], D. Wang[76], Y. Wang[76], Y. Wang[14], Z. Wang[76], A. Wegrzynek[3], F. Weiglhofer[11], S. C. Wenzel[3], J. P. Wessels[24], P. K. Wiacek[40], J. Wiechula[19], J. Wikne[31], G. Wilk[126], J. Wilkinson[12], G. A. Willems[24], B. Windelband[25], M. Winn[39], J. R. Wright[95], W. Wu[76], Y. Wu[36], K. Xiong[76], Z. Xiong[36], R. Xu[14], A. Yadav[110], A. K. Yadav[2], Y. Yamaguchi[93], S. Yang[79], S. Yang[18], S. Yano[93], E. R. Yeats[90], J. Yi[14], Z. Yin[14], I.-K. Yoo[61], J. H. Yoon[79], H. Yu[132], S. Yuan[18], A. Yuncu[25], V. Zaccolo[55], C. Zampolli[3], F. Zanone[25], N. Zardoshti[3], P. Závada[140], M. Zhalov[10], B. Zhang[25], C. Zhang[39], L. Zhang[76], M. Zhang[14,47], M. Zhang[14,78], S. Zhang[76], X. Zhang[14], Y. Zhang[36], Y. Zhang[36], Z. Zhang[14], M. Zhao[106], V. Zherebchevskii[10], Y. Zhi[106], D. Zhou[14], Y. Zhou[52], J. Zhu[14,26], S. Zhu[12,36], Y. Zhu[14], S. C. Zugravel[13] & N. Zurlo[62,63]

[1]INFN Sezione di Bari, Bari, Italy. [2]Variable Energy Cyclotron Centre, Homi Bhabha National Institute, Kolkata, India. [3]European Organization for Nuclear Research (CERN), Geneva, Switzerland. [4]Dipartimento di Fisica dell'Università and Sezione, INFN, Turin, Italy. [5]Dipartimento DISAT del Politecnico and Sezione, INFN, Turin, Italy. [6]Dipartimento di Fisica e Astronomia dell'Università and Sezione, INFN, Bologna, Italy. [7]Department of Physics, Aligarh Muslim University, Aligarh, India. [8]Korea Institute of Science and Technology Information, Daejeon, Republic of Korea. [9]Faculty of Science, P.J. Šafárik University, Košice, Slovak Republic. [10]Affiliated with an institute formerly covered by a cooperation agreement with CERN, Geneva, Switzerland. [11]Frankfurt Institute for Advanced Studies, Johann Wolfgang Goethe-Universität Frankfurt, Frankfurt, Germany. [12]Research Division and ExtreMe Matter Institute EMMI, GSI Helmholtzzentrum für Schwerionenforschung, Darmstadt, Germany. [13]INFN Sezione di Torino, Turin, Italy. [14]Central China Normal University, Wuhan, China. [15]Instituto de Fsica, Universidad Nacional Autónoma de México, Mexico City, Mexico. [16]University of Houston, Houston, TX, USA. [17]Sungkyunkwan University, Suwon City, Republic of Korea. [18]Department of Physics and Technology, University of Bergen, Bergen, Norway. [19]Institut für Kernphysik, Johann Wolfgang Goethe-Universität Frankfurt, Frankfurt, Germany. [20]Physik Department, Technische Universität München, Munich, Germany. [21]High Energy Physics Group, Universidad Autónoma de Puebla, Puebla, Mexico. [22]Horia Hulubei National Institute of Physics and Nuclear Engineering, Bucharest, Romania. [23]University of Derby, Derby, UK. [24]Institut für Kernphysik, Universität Münster, Münster, Germany. [25]Physikalisches Institut, Ruprecht-Karls-Universität Heidelberg, Heidelberg, Germany. [26]INFN Sezione di Padova, Padova, Italy. [27]INFN Sezione di Bologna, Bologna, Italy. [28]Lawrence Berkeley National Laboratory, Berkeley, CA, USA. [29]Laboratoire de Physique Subatomique et de Cosmologie, Université Grenoble-Alpes, CNRS-IN2P3, Grenoble, France. [30]Universidade de São Paulo (USP), São Paulo, Brazil. [31]Department of Physics, University of Oslo, Oslo, Norway. [32]Yale University, New Haven, CT, USA. [33]University of Tokyo, Tokyo, Japan. [34]INFN Sezione di Catania, Catania, Italy. [35]Gangneung-Wonju National University, Gangneung, Republic of Korea. [36]University of Science and Technology of China, Hefei, China. [37]Indian Institute of Technology Indore, Indore, India. [38]Physics Department, University of Jammu, Jammu, India. [39]IRFU Département de Physique Nucléaire (DPhN), Centre d'Etudes de Saclay (CEA), Université Paris-Saclay, Saclay, France. [40]AGH University of Krakow, Cracow, Poland. [41]University of Kansas, Lawrence, KS, USA. [42]Dipartimento Interateneo di Fisica, 'M. Merlin' and Sezione INFN, Bari, Italy. [43]National and Kapodistrian University of Athens, School of Science, Department of Physics, National and Kapodistrian University of Athens, Athens, Greece. [44]Department of Physics, Gauhati University, Guwahati, India. [45]HUN-REN Wigner Research Centre for Physics, Budapest, Hungary. [46]SUBATECH, IMT Atlantique, Nantes Université, CNRS-IN2P3, Nantes, France. [47]Université Clermont Auvergne, CNRS/IN2P3 LPC, Clermont-Ferrand, France. [48]Department of Physics, Lund University, Lund, Sweden. [49]Affiliated with an international laboratory covered by a cooperation agreement with CERN, Geneva, Switzerland. [50]Indian Institute of Technology Bombay (IIT), Mumbai, India. [51]Sección Fsica, Departamento de Ciencias, Pontificia Universidad Católica del Perú, Lima, Peru. [52]Niels Bohr Institute, University of Copenhagen, Copenhagen, Denmark. [53]Université de Strasbourg, CNRS, IPHC UMR 7178, Strasbourg, France. [54]Universidad Autónoma de Sinaloa, Culiacán, Mexico. [55]Dipartimento di Fisica dell'Università and Sezione, INFN, Trieste, Italy. [56]Physics Department, Panjab University, Chandigarh, India. [57]Faculty of Nuclear Sciences and Physical Engineering, Czech Technical University in Prague, Prague, Czech Republic. [58]Nuclear Physics Institute of the Czech Academy of Sciences, Husinec-Řež, Czech Republic. [59]Department of Physics and Centre for Astroparticle Physics and Space Science (CAPSS), Bose Institute, Kolkata, India. [60]Oak Ridge National Laboratory, Oak Ridge, TN, USA. [61]Department of Physics, Pusan National University, Pusan, Republic of Korea. [62]Università di Brescia, Brescia, Italy. [63]INFN Sezione di Pavia, Pavia, Italy. [64]Institute of Space Science (ISS), Bucharest, Romania. [65]Politecnico di Bari and Sezione INFN, Bari, Italy. [66]Faculty of Physics, Sofia University, Sofia, Bulgaria. [67]Nuclear Physics Group, STFC Daresbury Laboratory, Daresbury, UK. [68]Stefan Meyer Institut für Subatomare Physik (SMI), Vienna, Austria. [69]iThemba LABS, National Research Foundation, Somerset West, South Africa. [70]University of the Witwatersrand, Johannesburg, South Africa. [71]The Henryk Niewodniczanski Institute of Nuclear Physics, Polish Academy of Sciences, Cracow, Poland. [72]Dipartimento di Fisica 'E.R. Caianiello', Università degli Studi di Salerno and Gruppo Collegato INFN, Salerno, Italy. [73]Universitatea Nationala de Stiinta si Tehnologie Politehnica Bucuresti, Bucharest, Romania. [74]Warsaw University of Technology, Warsaw, Poland. [75]University of Liverpool, Liverpool, UK. [76]Fudan University, Shanghai, China. [77]Institut de Physique des 2 Infinis de Lyon, Université de Lyon, CNRS/IN2P3, Lyon, France. [78]Dipartimento di Fisica e Astronomia dell'Università and Sezione INFN, Padova, Italy. [79]Inha University, Incheon, Republic of Korea. [80]Saha Institute of Nuclear Physics, Homi Bhabha National Institute, Kolkata, India. [81]Nikhef National institute for Subatomic Physics, Amsterdam, The Netherlands. [82]University of Tsukuba, Tsukuba, Japan. [83]INFN Sezione di Cagliari, Cagliari, Italy. [84]School of Physics and Astronomy, University of Birmingham, Birmingham, UK. [85]IJCLab, Université Paris-Saclay, CNRS/IN2P3, Orsay, France. [86]Università del Piemonte Orientale, Vercelli, Italy. [87]Universidade Federal do ABC, Santo Andre, Brazil. [88]Dipartimento di Fisica, Università di Pavia, Pavia, Italy. [89]Dipartimento di Fisica dell'Università and Sezione, INFN, Cagliari, Italy. [90]Department of Physics, University of California Berkeley, Berkeley CA, USA. [91]Università degli Studi di Foggia, Foggia, Italy. [92]Faculty of Mathematics, Physics and Informatics, Comenius University Bratislava, Bratislava, Slovak Republic. [93]Physics Program and International Institute for Sustainability with Knotted Chiral Meta Matter (WPI-SKCM2), Hiroshima University, Hiroshima, Japan. [94]Laboratori Nazionali di Frascati, INFN, Frascati, Italy. [95]The University of Texas at Austin, Austin, TX, USA. [96]Sezione di Trieste, INFN, Trieste, Italy. [97]Saga University, Saga, Japan. [98]National Institute of Science Education and Research, Homi Bhabha National Institute, Jatni, India. [99]Chicago State University, Chicago, IL, USA. [100]Instituto de Física, Universidade Federal do Rio Grande do Sul (UFRGS), Porto Alegre, Brazil. [101]University of Tennessee, Knoxville, TN, USA. [102]Wayne State University, Detroit, MI, USA. [103]Faculty of Electrical Engineering, Mechanical Engineering and Naval Architecture, University of Split, Split, Croatia. [104]Institute for Gravitational and Subatomic Physics (GRASP), Utrecht University/Nikhef, Utrecht, Netherlands. [105]A.I. Alikhanyan National Science Laboratory (Yerevan Physics Institute) Foundation, Yerevan, Armenia. [106]China Nuclear Data Center, China Institute of Atomic Energy, Beijing, China. [107]Nagasaki Institute of Applied Science, Nagasaki, Japan. [108]Yonsei University, Seoul, Republic of Korea. [109]University of Jyväskylä, Jyväskylä, Finland. [110]Helmholtz-Institut für Strahlen- und Kernphysik, Rheinische Friedrich-Wilhelms-Universität Bonn, Bonn, Germany. [111]Faculty of Technology, Environmental and Social Sciences, Bergen, Norway. [112]Centro de Investigación y de Estudios Avanzados (CINVESTAV), Mexico City and Mérida, Mexico. [113]Fachbereich Informatik und Mathematik, Johann-Wolfgang-Goethe Universität Frankfurt Institut für Informatik, Frankfurt, Germany. [114]Ohio State University, Columbus OH, USA. [115]Technical University of Košice, Košice, Slovak Republic. [116]National Research and Innovation Agency - BRIN, Jakarta, Indonesia. [117]Universidade Estadual de Campinas (UNICAMP), Campinas, Brazil. [118]Instituto de Ciencias Nucleares, Universidad Nacional Autónoma de México, Mexico City, Mexico. [119]Suranaree University of Technology, Nakhon Ratchasima, Thailand. [120]Institute of Experimental Physics, Slovak Academy of Sciences, Košice, Slovak Republic. [121]Yildiz Technical University, Istanbul, Turkey. [122]Jeonbuk National University, Jeonju, Republic of Korea. [123]Department of Physics, Sejong University, Seoul, Republic of Korea. [124]California Polytechnic State University, San Luis Obispo CA, USA. [125]Physics Department, Faculty of Science, University of Zagreb, Zagreb, Croatia. [126]National Centre for Nuclear Research, Warsaw, Poland. [127]Dipartimento di Fisica e Astronomia dell'Università and Sezione INFN, Catania, Italy. [128]University of South-Eastern Norway, Kongsberg, Norway. [129]Centro de Aplicaciones Tecnológicas y Desarrollo Nuclear (CEADEN), Havana, Cuba. [130]Dipartimento di Scienze MIFT, Università di Messina, Messina, Italy. [131]Helsinki Institute of Physics (HIP), Helsinki, Finland. [132]Chungbuk National University, Cheongju, Republic of Korea. [133]China University of Geosciences, Wuhan, China. [134]Creighton University, Omaha, NE, USA. [135]National Nuclear Research Center, Baku, Azerbaijan. [136]Institute of Physics, Homi Bhabha National Institute, Bhubaneswar, India. [137]Physikalisches Institut, Eberhard-Karls-Universität Tübingen, Tübingen, Germany. [138]Nara Women's University (NWU), Nara, Japan. [139]Bogolyubov Institute for Theoretical Physics, National Academy of Sciences of Ukraine, Kiev, Ukraine. [140]Institute of Physics of the Czech Academy of Sciences, Prague, Czech Republic. [141]Present address: Max-Planck-Institut fur Physik, Munich, Germany. [142]Present address: Italian National Agency for New Technologies, Energy and Sustainable Economic Development (ENEA), Bologna, Italy. [143]Present address: Instituto de Fisica da Universidade de São Paulo, São Paulo, Brazil. [144]Present address: Dipartimento DET del Politecnico di Torino, Turin, Italy. [145]Present address: Department of Applied Physics, Aligarh Muslim University, Aligarh, India. [146]Present address: Institute of Theoretical Physics, University of Wroclaw, Wrocław, Poland. [147]Present address: Facultad de Ciencias, Universidad Nacional Autónoma de México, Mexico City, Mexico. [148]Deceased: R. C. Lemmon, A. Vasiliev.

Methods

Event selection

The results are based on the analysis of a dataset comprising inelastic pp collisions at $\sqrt{s}$ = 13 TeV, recorded with the ALICE detector[45,46] during the LHC run 2 (2015–2018). The events are selected using a high-multiplicity (HM) trigger, which captures the highest multiplicity events—specifically, the top 0.17% of all inelastic collisions that include at least one charged particle within the pseudorapidity interval $|\eta| < 1$ (denoted as 0.17% INEL > 0). This approach ensures a statistically rich sample, as a five-fold increase in the production of (anti)deuteron candidates has been observed in HM pp collisions compared with minimum bias pp collisions[47]. The sample of HM-triggered collisions considered for this analysis corresponds to 1×10^9 events. On average, 31 charged tracks are found within $|\eta| < 0.5$ (ref. 48) for the HM-triggered collisions. Detailed descriptions of the event selection criteria, pileup rejection techniques, primary-vertex reconstruction methods and the HM trigger procedure are provided in ref. 49.

Tracking and particle identification

Particle identification and momentum measurement of charged particles are performed using the inner tracking system (ITS)[50], time projection chamber (TPC)[51] and time-of-flight (TOF)[52] detectors of ALICE covering the whole azimuthal angle and the pseudorapidity interval $|\eta| < 0.9$. These detectors are located within a uniform magnetic field of 0.5 T along the beam axis, generated by the ALICE solenoid magnet, which causes the trajectories of particles to bend. The curvature of the charged-particle tracks is used to measure the particle momenta. The transverse momentum for pion and deuteron candidates is determined with a resolution ranging from approximately 2% for tracks with $p_T \approx 10$ GeV c^{-1} to below 1% for $p_T < 1$ GeV c^{-1}. Particle identification is performed by measuring the energy loss per unit track length (dE/dx) in the TPC detector and the particle velocity (β) in the TOF detector. For tracks in the TPC detector, the signal is obtained from the $n\sigma_{\mathrm{TPC}}$ distribution, where $n\sigma_{\mathrm{TPC}}$ represents the deviation of the measured signal from the expected value for a given particle hypothesis, normalized by the detector resolution. Similarly, for the TOF detector, the resolution is defined by $n\sigma_{\mathrm{TOF}}$, which quantifies the difference between the measured and expected time of flight, also normalized by the resolution. Further experimental details are discussed in ref. 46. The selection criteria for pion and deuteron tracks used in this work are described in refs. 30,41.

Pions are identified by the measurement of the specific energy loss within $|n\sigma_{\mathrm{TPC}}| < 3$ in a transverse momentum range $p_T \in [0.14, 4.0]$ GeV c^{-1}. This information is combined with the TOF measurement by taking the geometric sum, $\sqrt{n\sigma_{\mathrm{TPC}}^2 + n\sigma_{\mathrm{TOF}}^2} < 3$, for track momentum $p >$ 0.5 GeV c^{-1}. Similarly, the deuteron candidates are selected within a transverse momentum range $p_T \in [0.8, 2.4]$ GeV c^{-1}. They are identified by using $|n\sigma_{\mathrm{TPC}}| < 3$ for candidate tracks with momentum $p < 1.4$ GeV c^{-1}, whereas both TPC and TOF information are required, $\sqrt{n\sigma_{\mathrm{TPC}}^2 + n\sigma_{\mathrm{TOF}}^2} < 3$, for candidates with $p > 1.4$ GeV c^{-1}. Moreover, for (anti)deuteron candidate selections, electrons are rejected by the condition $n\sigma_{\mathrm{TPC,e}} > 6$ for $p < 1.4$ GeV c^{-1} and pions are rejected by the condition $n\sigma_{\mathrm{TPC},\pi} > 3$ for the tracks with momentum $p > 1.4$ GeV c^{-1}. Overall, using these methods, a purity of 99% for $\pi^{\pm}$ and 100% for (anti)deuterons is achieved.

The selection criteria of pions and deuterons constitute the primary source of systematic uncertainties associated with the measured correlation function. All particle selection criteria are varied from their default values. To account for the effect of possible correlations, the analysis of π^+–d and π^-–d pairs is repeated 44 times using random combinations of these selection criteria. The total systematic uncertainties are extracted by first randomly selecting a correlation function from the 44 systematic variations. For each sampled function, a bootstrap method is applied by randomly varying the $C(k^*)$ values in the individual k^* bins according to their statistical uncertainties, assuming Gaussian errors. This results in a distribution of values for each k^* bin, which is then fitted to determine the total uncertainty. As the statistical and systematic uncertainties are independent, the total uncertainty is obtained by adding them in quadrature. The systematic component is then determined by subtracting the known statistical uncertainty. The systematic uncertainties are largest at low $k^* \approx 10$ MeV c^{-1}, reaching 1%. The same procedure is applied to extract the uncertainties of the fitted parameters and propagated to the final results on the fraction of deuterons stemming from resonance-assisted fusion processes.

Characterization of the particle-emitting source

A standard approach to evaluate the source function, used by ALICE in pp collisions, is the resonance source model (RSM)[41,44]. In these publications, the ALICE Collaboration measured the source size for baryon–baryon, meson–baryon and meson–meson pairs, demonstrating a common emission source of all particles and resonances produced directly in the collision. These are described as primordial particles, whereas the short-lived resonances that decay into the pairs of interest on the timescale of fm c^{-1} will lead to an increase in the effective source size. If this increase in the source size is properly modelled by Monte Carlo simulations, the underlying primordial source has a Gaussian profile of width r_{core}, and scales as a function of the pair transverse mass $m_T = (k_T^2 + m^2)^{1/2}$, where m is the average mass, the average of the masses of the two particles constituting the pair and $k_T = |\mathbf{p}_{T,1} + \mathbf{p}_{T,2}|/2$ is the average transverse momentum of the pair[41,44]. The scaling of the primordial source size follows a power law $r_{\mathrm{core}} = a\langle m_T \rangle^b + c$, where the parameters for the high-multiplicity pp collisions at $\sqrt{s}$ = 13 TeV used for the present π–d analysis are provided in ref. 44. The knowledge of both the pair average m_T and the cocktail of contributing resonances allows us to evaluate both the r_{core} and subsequently the total source distribution $S(r^*)$. The present analysis incorporates the resonances decaying into pions from the ThermalFIST model[34,37], as already performed in the ALICE π–π and p–π analyses[38,41]. From the study of p–d and K^+–d correlations in pp collisions at $\sqrt{s}$ = 13 TeV (ref. 30), it has been shown that in pp collisions, the hadron–deuteron pairs follow the same transverse mass scaling as other hadron–hadron pairs, allowing to constrain the π–d emission source using the RSM. The deuterons are not produced directly by resonances. Nevertheless, the present work demonstrates that resonances decaying into nucleons are an important step in the production mechanism. This will lead to an effective delay in the deuteron production, an effect already described in a previous analysis of the K^+–d analysis[53]. The present analysis adopts a conservative approach and integrates two extreme scenarios for the deuteron production as part of the systematic uncertainties, namely, assuming either that all deuterons are primordial or that the deuteron formation is delayed based on the amount of emission delay by which their constituent nucleons are affected[44]. This variation, which affects the effective source size, r_{eff} of up to 0.08 fm, is included in the systematic uncertainties on the modelling of the correlation functions. The final values for the r_{eff}, after the inclusion of resonances, are summarized in the Extended Data Table 1, along with the total uncertainties.

Corrections of the correlation function

The experimental correlation function, defined as $C(k^*) = \mathcal{N}[N_{\mathrm{same}}(k^*)/N_{\mathrm{mixed}}(k^*)]$ is only corrected by a normalization constant $\mathcal{N}$, by ensuring that the correlation becomes unity for $k^* \in (400, 600)$ MeV c^{-1}. The remaining corrections are included in the fit function

$$C_{\mathrm{fit}}(k^*) = \varepsilon(k^*) \otimes B(k^*)[\lambda_{\mathrm{gen}} C_{\mathrm{gen}}(k^*) + (1-\lambda_{\mathrm{gen}})]. \quad (1)$$

The parameter $\varepsilon(k^*)$ incorporates momentum resolution effects, which are included by obtaining a transformation matrix that can be used to apply resolution effects to the correlation functions. Details on the procedure are provided in the supplemental materials in ref. 44. The required experimental inputs are the matrix itself and the

experimental mixed-event sample, both of which are provided in the HEPData entry related to this work. The baseline $B(k^*) = a + bk^{*2} + ck^{*3}$ accounts for any remaining long-range correlations[54]. These correlations do not contribute as an additive contamination to the correlations as misidentified particles do, but rather stem from the kinematics of the collision event. These long-range correlations are not correlated to the final-state interaction and can therefore be factorized and included as a multiplicative factor in the correlation. All the parameters of the baseline are left free in the fit procedure. The final correction to the correlation function is λ_{gen}, which represents the amount of genuine π–d pairs. In the context of the source, a genuine particle is either a primordial or the decay product of a short-lived resonance of lifetime $c\tau < 5$ fm c^{-1}. Details on the extraction of these parameters for the pions and deuterons are provided in ref. 41 and ref. 30, respectively. Combining the information for the two species, the correction obtained for $\pi^{\pm}$–d is summarized in Extended Data Table 1. The $(1 - \lambda_{\text{gen}})$ factor in the definition of $C_{\text{fit}}(k^*)$ reflects the remaining non-genuine correlations, which are assumed to produce a flat correlation signal. These non-genuine correlations stem from misidentified particles, as well as feed-down from long-lived resonances. Owing to the high purity in the present analysis, the non-genuine correlations are predominantly linked to the feed-down into pions from non-strong decays, such as decays of kaons[41]. There is no contribution to the non-genuine correlation from feed-down into deuterons, as these decay processes do not exist, except for the weak decay of the hypertriton ($^3_\Lambda\text{H} \rightarrow \pi^- + \text{p} + \text{d}$), which has a negligible effect.

Spectral shape of Δ

In the measurement of the $\pi^{\pm}$–p correlation functions[38], a prominent peak around $k^* = 211$ MeV c^{-1} can be seen, associated with the Δ resonances (Δ^{++} for π^+–p and Δ^0 for π^-–p). In the decay of a Δ resonance into a pion–nucleon pair, the Δ is at rest in the centre-of-mass frame of the decay products. By applying energy and momentum conservation for this two-body decay, the invariant mass of the Δ is related to the relative momentum k^* of the decay products by

$$m_\Delta = \sqrt{(k^*)^2 + m_\pi^2} + \sqrt{(k^*)^2 + m_N^2}. \tag{2}$$

Inverting this expression yields the expected relative momentum k^* associated with a given Δ mass

$$k^* = \frac{\sqrt{(m_\Delta^2 - m_\pi^2 - m_N^2)^2 - 4m_\pi^2 m_N^2}}{2m_\Delta}. \tag{3}$$

For the nominal Δ mass of $M_\Delta = 1.215$ GeV c^{-2}, this corresponds to a relative momentum of $k^* = 211$ MeV c^{-1} for the pion–nucleon pair. The peak position observed in the $\pi^{\pm}$–p correlations is shifted to lower values than the nominal Δ mass because of the rescattering of the decay products and regeneration of the resonances[55–57].

Following ref. 38, the Δ spectral shape is modelled as $C_\Delta(k^*) = \mathcal{N}_\Delta \times PS(p_{\text{T},\Delta}, T) \times Sill(M_\Delta, \Gamma_\Delta)$. The first term $\mathcal{N}_\Delta$ is a normalization constant, whereas the undisturbed spectral shape of the resonances is described usingthe Sill distribution[58], which depends on the resonance mass M_Δ and width Γ_Δ. As the *Sill* is expressed as a function of k^*, it is essential to account for the Jacobian factor $|\mathrm{d}m_\Delta/\mathrm{d}k^*|$ in the change of variables, where m_Δ is given by equation (2). Modifications of the spectral shape due to rescattering and resonance regeneration effects are incorporated by a multiplicative $PS(p_{\text{T},\Delta}, T)$ term[56,57], a Boltzmann-like phase space factor,

$$PS(p_{\text{T},\Delta}, T) \propto \frac{M}{\sqrt{M^2 + p_{\text{T},\Delta}^2}} \exp\left[-\frac{\sqrt{M^2 + p_{\text{T},\Delta}^2}}{T}\right], \tag{4}$$

acting as a weight for the emission of the resonance with certain transverse momentum $p_{\text{T},\Delta}$ at a temperature T. The latter is referred to as the 'Δ spectral temperature' in ref. 38.

To obtain the corresponding spectral shape in the π–d correlation, a simple approach is adopted by assuming that each measured deuteron consists of two nucleons of equal momenta. In this way, the Δ spectral shape in the π–N system (equation (3)) can be transformed into the π–d PRF. For a nominal Δ mass of $M_\Delta = 1.215$ GeV c^{-2} leads to $k^* = 237$ MeV c^{-1} in the pion–deuteron system.

A final systematic check was performed by allowing a non-zero relative momentum between the two nucleons forming a deuteron. For this, a relative momentum sampled from a distribution, which was obtained from a coalescence model[59], was used. The relative momentum is, on average, about 100 MeV c^{-1} (ref. 59). The final shape of the Δ peak in the π–d correlation remains identical regardless of the assumption of the relative momenta between the nucleons. Thus, the simpler approach of identical nucleon momenta was used in the analysis.

Fitting the π–d correlation

The fit function is defined by equation (1). The genuine correlation $C_{\text{gen}}(k^*)$ encapsulates Coulomb and strong interactions alongside contributions from the Δ resonance. The interaction components were modelled using the CATS framework[42], which uses the Schrödinger equation and requires as input the source function and the strong interaction potential. The contribution of the strong interaction is minimal because of the small scattering parameters of the π–d system, as the scattering length is cancelled for π–p and π–n pairs[32,33]. The real part of the π^-–d potential was included in the fit[32,33]. To account for the Δ resonance, a phenomenological approach was adopted, expressing the genuine correlation as

$$C_{\text{gen}}(k^*) = C_{\text{interaction}}(k^*)[F_\Delta \mathcal{A}_\Delta C_\Delta(k^*) + (1 - F_\Delta \mathcal{A}_\Delta)], \tag{5}$$

where F_Δ is a free parameter representing the number of Δ resonances contributing to deuteron production divided by the number of all measured deuterons. The parameter $\mathcal{A}_\Delta$ is an arbitrary normalization constant, introduced to keep the physically motivated definition of F_Δ intact. The term $C_\Delta(k^*)$ reflects the spectral shape of the Δ resonance measured and fitted in the π–p analysis by ALICE (see previous section)[38], transformed to the π–d system. The mass ($M_\Delta = 1{,}215$ MeV c^{-2}) and width (Γ_Δ) of the Δ resonance in the present analysis are fixed to the values extracted from the measured π–p correlations, whereas the Δ spectral temperature T is fitted. The width Γ_Δ is dependent on m_{T}, for the m_{T}-integrated data shown in Fig. 2, the value is 95 MeV c^{-2}.

The fit to the data is performed in the range $k^* \in (0, 500)$ MeV c^{-1}, with a systematic variation of $k^* \in (0, 600)$ MeV c^{-1}. As a systematic check, a 5% variation in λ_{gen} is considered, accounting for the uncertainties arising in the determination of secondary contributions and purities due to systematic variations in the particle candidate selection criteria. As the parameters F_Δ and $\mathcal{A}_\Delta$ are maximally correlated, the fit is performed using the effective parameter $F'_\Delta = F_\Delta \mathcal{A}_\Delta$. The parameter F'_Δ represents the fraction of π–d pairs in which the pion and at least one of the nucleons within the deuteron originate from a Δ. This can be expressed as

$$F'_\Delta = \int C_\Delta(k^*) N_{\text{mixed}}(k^*) \mathrm{d}k^* \Big/ \int N_{\text{mixed}}(k^*) \mathrm{d}k^*. \tag{6}$$

As the key parameter in this study is F_Δ, establishing a relationship with F'_Δ is necessary. A straightforward analytical transformation can be derived under the assumption that most recorded collisions containing a reconstructed deuteron include only one. This implies that no additional Δ signal is introduced in the peak region because of combinatorial effects, and the number of Δ resonances associated with deuteron production becomes equal to the number of pairs (peak amplitude) linked to a Δ. This results in

$$F_\Delta \approx \int C_\Delta(k^*) N_{\mathrm{mixed}}(k^*)\mathrm{d}k^*/N_\mathrm{d}, \quad (7)$$

where N_d is the total number of reconstructed deuterons used in the analysis. Given the fraction of events containing more than one deuteron, the uncertainty associated to equation (7) is estimated to be negligible ($\lesssim$0.03%). Using equations (6) and (7)

$$F_\Delta = \frac{\int N_{\mathrm{mixed}}(k^*)}{N_\mathrm{d}} F'_\Delta = 0.533 \pm 0.035, \quad (8)$$

where both $N_{\mathrm{mixed}}(k^*)$ and N_d are measured, whereas F'_Δ is extracted from the fit. The quoted uncertainty combines the statistical and systematic errors of the data and the fit. The fit results for the phase space parameters (equation (4)) are $p_{\mathrm{T},\Delta} = 985 \pm 171$ MeV c^{-1} and $T = 20 \pm 2$ MeV.

Deuteron and proton fraction from resonances

Relating F_Δ to the probability P_Δ of producing a single nucleon from a Δ resonance requires accounting for the reconstruction efficiency. Although the efficiency of deuterons cancels out because of the definition of F_Δ, the pion reconstruction efficiency, ε_π, must be included. The pion efficiencies are obtained using Monte Carlo simulations produced with PYTHIA 8.2 (ref. 60), tuned to reproduce pp collisions at 13 TeV, and filtered through the ALICE detector and reconstruction algorithm[45].

The following calculations are based purely on combinatorial considerations, without explicitly accounting for the microscopic or kinematical properties of the resonances. The probability of producing exactly one of the two nucleons within the deuteron from a Δ resonance and detecting the decay pion is $2\varepsilon_\pi P_\Delta(1 - P_\Delta)$. The probability of having both nucleons within the deuteron originating from a Δ resonance and detecting both decay pions is $\varepsilon_\pi^2 P_\Delta^2$, whereas the probability for the same production scenario when failing to detect one of the pions is $2\varepsilon_\pi(1 - \varepsilon_\pi)P_\Delta^2$. Note that in the case in which both nucleons in the deuteron stem from a Δ, the final state contains a single deuteron and two pions, resulting in two entries in the peak region of the correlation function. As F_Δ is defined as the ratio of the number of π–d pairs to single deuterons, the corresponding term, $\varepsilon_\pi^2 P_\Delta^2$, contributes with twice the number of pairs. Taking all these considerations into account and adding all of the terms together leads to

$$F_\Delta = 2\varepsilon_\pi P_\Delta. \quad (9)$$

Owing to the effect of double counting some of the pairs, the result must be transformed into the fraction of (single) deuterons, f_Δ, produced by a Δ resonance. The definition of f_Δ is similar to F_Δ, but it removes the double-counting effect by taking the pure term $\varepsilon_\pi^2 P_\Delta^2$ without additional multiplication by 2. This leads to the expression

$$f_\Delta = 2\varepsilon_\pi P_\Delta\left(1 - \frac{\varepsilon_\pi P_\Delta}{2}\right). \quad (10)$$

Equations (9) and (10) account for the pion reconstruction efficiency, ε_π, in correcting the single-particle purities. Consequently, f_Δ is evaluated after applying this efficiency correction. The efficiency-independent result, f_Δ^{true}, is obtained by setting $\varepsilon_\pi = 1$ and expressing it in terms of the measured F_Δ

$$f_\Delta^{\mathrm{true}} = 2P_\Delta\left(1 - \frac{P_\Delta}{2}\right) = \frac{F_\Delta}{\varepsilon_\pi}\left(1 - \frac{F_\Delta}{4\varepsilon_\pi}\right). \quad (11)$$

Considering the experimental result $F_\Delta = 0.533 \pm 0.035$ and a pion reconstruction efficiency of $\varepsilon_\pi = 71.53 \pm 0.65$%, evaluated using Monte Carlo simulation and averaged over the transverse momentum range for the pion candidates considered in the analysis, the true fraction is calculated as $f_\Delta^{\mathrm{true}} = 60.6 \pm 4.1$% The uncertainty is propagated by treating the errors of F_Δ and ε_π as independent.

It should be noted that this value must be considered a lower limit, as it is possible for the pion from the Δ decay to escape the detector acceptance, while the associated nucleus is still reconstructed. This loss of Δ resonances can be estimated only in a model-dependent manner using Monte Carlo event generators. Using EPOS 3 and PYTHIA 8.3, the loss of Δ particles due to η acceptance effects of the pion is estimated to be 15.5 ± 0.5%, implying that the value of F_Δ is underestimated by a similar amount. This number is obtained by calculating the acceptance as a function of k^* folded with the measured k^* distribution of the delta resonance. Re-evaluating f_Δ^{true} using equation (11) by including in addition the acceptance effect, the result becomes $f_\Delta^{\mathrm{true}} = 68.7 \pm 4.6$%.

Similar relations apply to deuterons produced from any resonance. However, the corresponding value is experimentally inaccessible because of the large spectral widths and small individual contributions of the other resonances. By defining the total fraction as f_R and assuming that the ratio $f_\Delta/f_\mathrm{R} = 0.773 \pm 0.012$, as predicted by the CSM models, holds for the experimental data, it is possible to extrapolate the acceptance corrected f_Δ^{true} to $f_\mathrm{R}^{\mathrm{true}} = 88.9 \pm 6.3$%.

The fraction of deuterons from Δ resonances was also obtained using the EPOS event generator. For this, all resonances included in EPOS were reweighted using the CSM ThermalFIST with the settings shown in the Extended Data Table 2. The deuteron formation is simulated using a coalescence afterburner[25] in which the information about the mother particles of the nucleons is conserved. For each nucleon in the deuteron, the potential resonance mother is identified and it is checked, whether the nucleon and the corresponding π fall within the p_T and η acceptance. If at least one nucleon in the deuteron fulfils this criterion, the deuteron is counted as stemming from a resonance. Finally, the η-acceptance of π is expected to be different in EPOS compared with the measurement, as the spectral shape of the Δ in the experiment is shifted towards lower k^* values. Losses due to this η-acceptance increase for increasing k^*, and thus are lower in reality than in the simulation. For this, the acceptance as a function of k^* is averaged using the experimental Δ spectral shape. The resulting acceptance is 83.6%, whereas a similar study with PYTHIA 8.3 gives 85.4%. Averaging these values and taking the variance as an uncertainty, the Monte Carlo yields $f_\Delta^{\mathrm{true,MC}} = 53.8 \pm 3.1$%, a result compatible with the experimental value of 60.6 ± 4.1%.

Although removing the model dependence of this estimation is not feasible, a validation can be performed using π–p correlation measurements[38]. For this purpose, we define the experimental fraction

$$F_{\Delta\to\mathrm{p,exp.}} = Y_{\mathrm{exp}}(\Delta)/[Y_{\mathrm{exp}}(\mathrm{p})\varepsilon_\pi] \quad (12)$$

for the π–p correlation function, where Y_{exp} denotes the experimentally measured yields of Δ and proton candidates. $Y_{\mathrm{exp}}(\Delta)$ is derived from the spectral shape $R_\Delta(k^*)$ published in ref. 38, and the proton–pion mixed-event distribution $N_{\mathrm{mixed,p-}\pi^\pm}$ using the relation

$$Y_{\mathrm{exp}}(\Delta) = \int R_\Delta(k^*) N_{\mathrm{mixed,p-}\pi^\pm}\mathrm{d}k^*. \quad (13)$$

This yields proton fractions of (14.2 ± 0.4)% from Δ^{++} decays and (5.8 ± 0.3)% from Δ^0 decays. The performance of the Monte Carlo event generators has been validated by calculating the corresponding model-based fraction $F_{\Delta\to\mathrm{p,MC}}$, using ThermalFIST to fix the initial yields of resonances and baryons, followed by PYTHIA or EPOS simulations within the ALICE acceptance. The change in the η-acceptance of the pion due to the shift of the experimentally observed Δ spectral shape is accounted for as described above. With this, ThermalFIST + EPOS predicts that 13.4% of the protons stem from Δ^{++} within the experimental acceptance and 4.6% from Δ^0. The corresponding numbers in ThermalFIST + PYTHIA are 14.6% for Δ^{++} and 5.0% for Δ^0.

Simulations

The simulation of the π^+–d correlation function was performed for three different hypotheses. The first simulation (Fig. 1c) is done using the EPOS 3 event generator combined with a coalescence afterburner developed in ref. 25, and it is able to reproduce the total number of deuterons in the analysed dataset without any free parameters. The deuterons obtained from this coalescence afterburner are combined with all pions of the desired charge in the same event to create the same-event distribution and with a buffer of up to 50 pions from previous events to build the mixed-event distribution. The predictions using ThermalFIST use the ThermalFIST sampler[34,61], which uses a Cooper-Frye particlization sampling procedure[61] and a blast-wave parameterization[62] tuned to pp collisions at $\sqrt{s}$ = 13 TeV (ref. 2) to obtain positions and momenta of the particles. In the blast-wave model, a thermalized medium expands radially with a subsequent instantaneous freeze-out. Its main parameters are the average expansion velocity $\langle\beta\rangle$, its kinetic freeze-out temperature T_{kin} and the velocity profile exponent n. ThermalFIST can directly produce deuterons without the need for an afterburner, and the same mixed events can be directly constructed in a similar manner as before. The last prediction obtained with ThermalFIST and SMASH uses the particles output by the ThermalFIST sampler in the kinematic region $|\eta| < 1$, including deuterons, and feeds it into the hadronic afterburner SMASH[35]. Inside SMASH, particles rescatter for up to 15 fm c^{-1} with a fixed timestep of Δt = 0.001 fm c^{-1}. The stochastic collision criterion is chosen to enable deuteron production and destruction using the $3 \leftrightarrow 2$ scattering processes such as $p + n + \pi \leftrightarrow d + \pi$. Furthermore, all $2 \leftrightarrow 2$ processes included in SMASH are enabled. The parameters used in ThermalFIST and the blast-wave model are shown in Extended Data Table 2.

Resonance spectral temperature

The modifications of the Δ spectral shape in the fitting procedure are modelled with the *PS* term presented in equation (4). As discussed above, this function is effectively controlled by the Δ spectral temperature T. The Δ spectral temperatures for the $\pi^{\pm}$–d system are shown in the Extended Data Fig. 1 as a function of the transverse mass, m_{T}, of one nucleon in the deuteron and the pion. They are comparable for π^+–d and π^-–d but differ from the $\pi^{\pm}$–p systems discussed in ref. 38, being lower than the spectral temperature found for Δ^{++} and higher than that of Δ^0. This aligns qualitatively with the resonance regeneration, $\Delta \leftrightarrow N\pi$, and rescattering picture[56,57]. For π^+–p, repulsive strong and Coulomb interactions stop Δ^{++} regeneration and rescattering earlier, whereas the attractive π^-–p interaction allows extended Δ^0 regeneration and rescattering, leading to a lower Δ spectral temperature. In π^+–d, the signal arises from $\Delta^{++} \rightarrow \pi^+$p (with subsequent fusion with a neutron) or $\Delta^+ \rightarrow \pi^+$n (with later fusion with a proton). As π^+–p interactions are repulsive and π^+–n interactions attractive[63], Δ^+ undergoes longer regeneration cycles than Δ^{++}. This results in a lower spectral temperature than a pure Δ^{++} as reflected in the data. Similarly, the π^-–d system includes contributions from $\Delta^0 \rightarrow \pi^-$p (attractive) and $\Delta^- \rightarrow \pi^-$n (repulsive). The shorter regeneration phase of Δ^- compared with Δ^0 yields a higher temperature for π^-–d than a pure π^-–p system, again seen in the measurements.

Dibaryon hypothesis and π–d correlations

Although no dibaryon states have been confirmed unambiguously (such as a bound NΔ), candidates have been proposed to explain anomalies in data reported by WASA-at-COSY[64], ELPH[65] and BGOOD[66]. In particular, the NΔ(2114) candidate was first observed by ELPH with a reported mass of $m_{2\mathrm{B}}$ = 2,140 MeV c^{-2}, and later by BGOOD at $m_{2\mathrm{B}}$ = 2,114 MeV c^{-2}. The expected imprint of such a state on the $\pi^{\pm}$–d correlation can be evaluated using ThermalFIST. Assuming an extreme upper limit of 100% for the unknown π–d branching ratio, as much as 28.5 ± 1.5% of deuterons could originate from this decay. Adopting a more realistic branching ratio, estimated from the ratio of elastic to inelastic π–d cross-sections[67], reduces this fraction to only 9.5 ± 0.5%, far below the 60.6 ± 4.1% estimated in the present study. Furthermore, if this small contribution is taken as a template, the fit to the data is incompatible with the observed correlation. When the amplitude is left unconstrained, the measured signal remains consistent with at most 1% of deuterons being produced through these decays. Hence, the experimental data strongly disfavour dibaryon decays as a notable source of the observed signal in the measured $\pi^{\pm}$–d correlation.

Data availability

This study has associated data in a HEPData repository at https://www.hepdata.net/record/ins2907586.

Code availability

This study has associated code/software in a data repository. The code/software used for the analysis is publicly available at GitHub (https://github.com/alisw/AliRoot, https://github.com/alisw/AliPhysics and https://github.com/dimihayl/DLM/tree/master/CATS).

45. ALICE Collaboration. The ALICE experiment at the CERN LHC. *J. Instrum.* **3**, S08002 (2008).
46. ALICE Collaboration. Performance of the ALICE experiment at the CERN LHC. *Int. J. Mod. Phys.* **A29**, 1430044 (2014).
47. ALICE Collaboration. Production of light (anti)nuclei in pp collisions at √s=13 TeV. *J. High Energy Phys.* **2022**, 106 (2022).
48. ALICE Collaboration. Unveiling the strong interaction among hadrons at the LHC. *Nature* **588**, 232–238 (2020).
49. ALICE Collaboration. Investigation of the p-Σ^0 interaction via femtoscopy in pp collisions. *Phys. Lett. B* **805**, 135419 (2020).
50. ALICE Collaboration. Alignment of the ALICE inner tracking system with cosmic-ray tracks. *J. Instrum.* **5**, P03003 (2010).
51. ALICE Collaboration. The ALICE TPC, a large 3-dimensional tracking device with fast readout for ultra-high multiplicity events. *Nucl. Instrum. Methods Phys. Res. A* **622**, 316–367 (2010).
52. Akindinov, A. et al. Performance of the ALICE time-of-flight detector at the LHC. *Eur. Phys. J. Plus* **128**, 44 (2013).
53. Vázquez Doce, O., Mihaylov, D. L. & Fabbietti, L. Study of the deuterons emission time in pp collisions at the LHC via kaon-deuteron correlations. *Eur. Phys. J. A* **61**, 53 (2025).
54. ALICE Collaboration. Exploring the NΛ–NΣ coupled system with high precision correlation techniques at the LHC. *Phys. Lett. B* **833**, 137272 (2022).
55. STAR Collaboration. Hadronic resonance production in d+Au collisions at $\sqrt{s_{\mathrm{NN}}}$=200 GeV measured at the BNL Relativistic Heavy Ion Collider. *Phys. Rev. C* **78**, 044906 (2008).
56. Reichert, T., Hillmann, P., Limphirat, A., Herold, C. & Bleicher, M. Delta mass shift as a thermometer of kinetic decoupling in Au+Au reactions at 1.23 AGeV. *J. Phys. G* **46**, 105107 (2019).
57. Reichert, T. & Bleicher, M. Kinetic mass shifts of ρ(770) and K^*(892) in Au+Au reactions at E_{beam}=1.23 AGeV. *Nucl. Phys. A* **1028**, 122544 (2022).
58. Giacosa, F., Okopińska, A. & Shastry, V. A simple alternative to the relativistic Breit–Wigner distribution. *Eur. Phys. J. A* **57**, 336 (2021).
59. Mahlein, M., Pinto, C. & Fabbietti, L. ToMCCA: a Toy Monte Carlo Coalescence Afterburner. *Eur. Phys. J. C* **84**, 1136–11 (2024).
60. Sjöstrand, T. et al. An introduction to PYTHIA 8.2. *Comput. Phys. Commun.* **191**, 159–177 (2015).
61. Vovchenko, V. et al. Proton number cumulants and correlation functions in Au-Au collisions at $\sqrt{s_{\mathrm{NN}}}$=7.7–200 GeV from hydrodynamics. *Phys. Rev. C* **105**, 014904 (2022).
62. Schnedermann, E. et al. Thermal phenomenology of hadrons from 200A GeV S+S collisions. *Phys. Rev. C* **48**, 2462–2475 (1993).
63. Hoferichter, M., Ruiz de Elvira, J., Kubis, B. & Meißner, U.-G. Roy–Steiner-equation analysis of pion–nucleon scattering. *Phys. Rep.* **625**, 1–88 (2016).
64. WASA-at-COSY Collaboration. Abashian-Booth-Crowe effect in basic double-pionic fusion: a new resonance? *Phys. Rev. Lett.* **106**, 242302 (2011).
65. Ishikawa, T. et al. Non-strange dibaryons studied in the $\gamma d \rightarrow \pi^0\pi^0 d$ reaction. *Phys. Lett. B* **789**, 413–418 (2019).
66. Jude, T. C. et al. Evidence of a dibaryon spectrum in coherent $\pi^0\pi^0$d photoproduction at forward deuteron angles. *Phys. Lett. B* **832**, 137277 (2022).
67. Particle Data Group Collaboration. Review of particle physics. *Prog. Theor. Exp. Phys.* **2022**, 083C01 (2022).

Acknowledgements We thank E. Bratkovskaya, J. Aichelin, K. Sun, A. Kievsky, M. Viviani, C.-M. Ko, S. Mrówczński, and S. König for the fruitful discussions on the pion–deuteron interactions and light (anti)nuclei production. We thank all its engineers and technicians for their invaluable contributions to the construction of the experiment and the CERN accelerator teams for the outstanding performance of the LHC complex. We gratefully acknowledge the resources and support provided by all Grid centres and the Worldwide LHC Computing Grid (WLCG) collaboration. We acknowledge the following funding agencies for their support in building and running the ALICE detector: A. I. Alikhanyan National Science Laboratory (Yerevan Physics Institute) Foundation (ANSL), State Committee of Science and World Federation of Scientists

(WFS), Armenia; Austrian Academy of Sciences, Austrian Science Fund (FWF): [M 2467-N36] and Nationalstiftung für Forschung, Technologie und Entwicklung, Austria; Ministry of Communications and High Technologies, National Nuclear Research Center, Azerbaijan; Conselho Nacional de Desenvolvimento Científico e Tecnológico (CNPq), Financiadora de Estudos e Projetos (Finep), Fundação de Amparo à Pesquisa do Estado de São Paulo (FAPESP) and Universidade Federal do Rio Grande do Sul (UFRGS), Brazil; Bulgarian Ministry of Education and Science, within the National Roadmap for Research Infrastructures 2020-2027 (object CERN), Bulgaria; Ministry of Education of China (MOEC), Ministry of Science & Technology of China (MSTC) and National Natural Science Foundation of China (NSFC), China; Ministry of Science and Education and Croatian Science Foundation, Croatia; Centro de Aplicaciones Tecnológicas y Desarrollo Nuclear (CEADEN), Cubaenergía, Cuba; Ministry of Education, Youth and Sports of the Czech Republic, Czech Republic; The Danish Council for Independent Research | Natural Sciences, the VILLUM FONDEN and Danish National Research Foundation (DNRF), Denmark; Helsinki Institute of Physics (HIP), Finland; Commissariat à l'Energie Atomique (CEA) and Institut National de Physique Nucléaire et de Physique des Particules (IN2P3) and Centre National de la Recherche Scientifique (CNRS), France; Bundesministerium für Bildung und Forschung (BMBF) and GSI Helmholtzzentrum für Schwerionenforschung GmbH, Germany; General Secretariat for Research and Technology, Ministry of Education, Research and Religions, Greece; National Research, Development and Innovation Office, Hungary; Department of Atomic Energy Government of India (DAE), Department of Science and Technology, Government of India (DST), University Grants Commission, Government of India (UGC) and Council of Scientific and Industrial Research (CSIR), India; National Research and Innovation Agency – BRIN, Indonesia; Istituto Nazionale di Fisica Nucleare (INFN), Italy; Japanese Ministry of Education, Culture, Sports, Science and Technology (MEXT) and Japan Society for the Promotion of Science (JSPS) KAKENHI, Japan; Consejo Nacional de Ciencia (CONACYT) y Tecnología, through Fondo de Cooperación Internacional en Ciencia y Tecnología (FONCICYT) and Dirección General de Asuntos del Personal Academico (DGAPA), Mexico; Nederlandse Organisatie voor Wetenschappelijk Onderzoek (NWO), the Netherlands; The Research Council of Norway, Norway; Pontificia Universidad Católica del Perú, Peru; Ministry of Science and Higher Education, National Science Centre and WUT ID-UB, Poland; Korea Institute of Science and Technology Information and National Research Foundation of Korea (NRF), Republic of Korea; Ministry of Education and Scientific Research, Institute of Atomic Physics, Ministry of Research and Innovation and Institute of Atomic Physics and Universitatea Nationala de Stiinta si Tehnologie Politehnica Bucuresti, Romania; Ministerstvo skolstva, vyskumu, vyvoja a mladeze SR, Slovakia; National Research Foundation of South Africa, South Africa; Swedish Research Council (VR) and Knut & Alice Wallenberg Foundation (KAW), Sweden; European Organization for Nuclear Research, Switzerland; Suranaree University of Technology (SUT), National Science and Technology Development Agency (NSTDA) and National Science, Research and Innovation Fund (NSRF via PMU-B B05F650021), Thailand; Turkish Energy, Nuclear and Mineral Research Agency (TENMAK), Turkey; National Academy of Sciences of Ukraine, Ukraine; Science and Technology Facilities Council (STFC), United Kingdom; National Science Foundation of the United States of America (NSF) and US Department of Energy, Office of Nuclear Physics (DOE NP), the United States. Moreover, individual groups or members have received support from Czech Science Foundation (grant no. 23-07499S), Czech Republic; FORTE project, reg. no. CZ.02.01.01/00/22_008/0004632, Czech Republic, co-funded by the European Union, Czech Republic; European Research Council (grant no. 950692), European Union; Deutsche Forschungs Gemeinschaft (DFG, German Research Foundation) 'Neutrinos and Dark Matter in Astro- and Particle Physics' (grant no. SFB 1258), Germany; ICSC - National Research Center for High Performance Computing, Big Data and Quantum Computing and FAIR – Future Artificial Intelligence Research, funded by the NextGenerationEU program (Italy); The National Recovery and Resilience Plan of the Republic of Bulgaria (project no. SUMMIT BG-RRP-2.004-0008-C01), funded by the European Union - NextGenerationEU (Bulgaria).

Author contributions The work reported in this document is the result of the ALICE Collaboration effort.

Competing interests The authors declare no competing interests.

Additional information

Correspondence and requests for materials should be addressed to The ALICE Collaboration.

Peer review information *Nature* thanks Kai-Jia Sun and the other anonymous reviewer for their contribution to the peer review of this work.

Reprints and permissions information is available at http://www.nature.com/reprints.

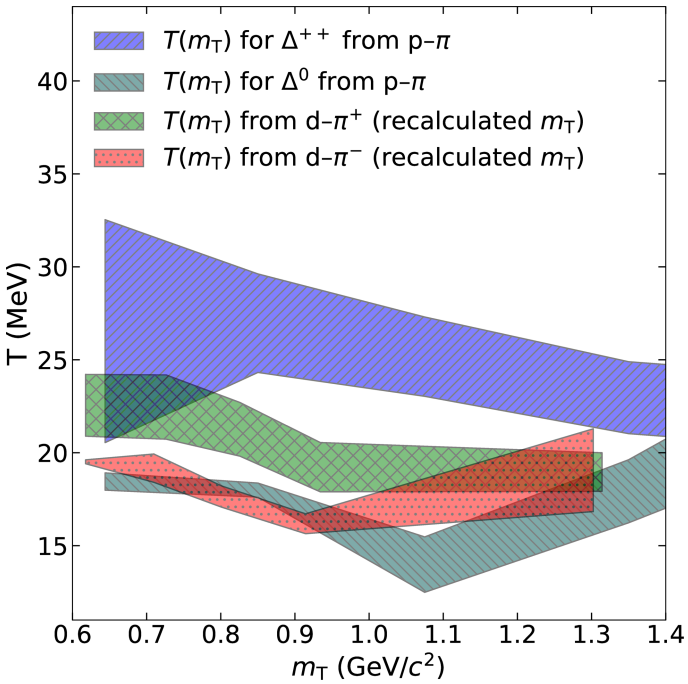

Extended Data Fig. 1 | Extracted Δ spectral temperature. The Δ spectral temperature is derived from $\pi^{\pm}$–p and $\pi^{\pm}$–d correlation functions measured in high-multiplicity pp collisions at $\sqrt{s} = 13$ TeV. The bands correspond to the uncertainties obtained by fits to the correlation functions, incorporating systematic uncertainties on the measured data, as well as those arising from variations in the source size and the λ parameter for the genuine interaction.

Extended Data Table 1 | Parameters used in the measured correlation function

m_T interval	m_T range (GeV/c^2)	$\langle m_T \rangle$ (GeV/c^2)	$r_{core}^{\pi^{\pm}\text{–d}}$ (fm)	$r_{eff}^{\pi^{\pm}\text{–d}}$ (fm)	$\lambda_{gen}^{\pi^{\pm}\text{–d}}$
integrated	$1.03 - 2.24$	1.27	1.08 ± 0.04	1.51 ± 0.12	81.6%

The values of the measured average transverse mass $\langle m_T \rangle$, extracted source sizes r_{core}, r_{eff}, and λ parameter which serves as the weights for the contribution of the genuine π^+ – d and π^- – d pairs in the measured correlation function.

Extended Data Table 2 | Parameters used in the π^+–d correlation function predictions for thermal production

Parameter	Value	Unit		Parameter	Value	Unit
$\langle\beta\rangle$	0.51	–		T_c	0.165	GeV
T_{kin}	0.16	GeV		μ_B	0	–
n	1.4	–		γ_S	0.85	–
η_{max}	1.5	–		$\mathrm{d}V/\mathrm{d}y$	75	fm^3
R_0	1.8	fm		V_c	3	$\mathrm{d}V/\mathrm{d}y$
Ref.	[2]	–	Ref.	[23]	–	

Parameters on the left side are used for the Blast-Wave parameterization, and parameters on the right are used for the ThermalFIST yields.